Western Graduate&PostdoctoralStudies

Western University
Scholarship@Western

Electronic Thesis and Dissertation Repository

8-21-2017 12:00 AM

Additive Manufacturing Process of 3D Polyaniline Transducers via Direct Ink Writing

Frederick Benjamin Holness
The University of Western Ontario

Supervisor
Aaron Price
The University of Western Ontario

Graduate Program in Mechanical and Materials Engineering
A thesis submitted in partial fulfillment of the requirements for the degree in Master of Engineering Science
© Frederick Benjamin Holness 2017

Follow this and additional works at: https://ir.lib.uwo.ca/etd

Part of the Electro-Mechanical Systems Commons, Manufacturing Commons, and the Polymer and Organic Materials Commons

Recommended Citation

Holness, Frederick Benjamin, "Additive Manufacturing Process of 3D Polyaniline Transducers via Direct Ink Writing" (2017). *Electronic Thesis and Dissertation Repository*. 4849.
https://ir.lib.uwo.ca/etd/4849

This Dissertation/Thesis is brought to you for free and open access by Scholarship@Western. It has been accepted for inclusion in Electronic Thesis and Dissertation Repository by an authorized administrator of Scholarship@Western. For more information, please contact wlswadmin@uwo.ca.

Abstract

Electroactive polymers exhibit a change in properties, typically size or shape, in response to electrical stimuli. One class of electroactive polymer of particular interest are the conjugated polymers, whose conjugated backbone structure imparts electrical conductivity. However, this structure imposes processing limitations restricting their form to 2D structures. To overcome this, we develop specially formulated polyaniline-based blends via counter-ion induced thermal doping for the fabrication of 3D conductive structures via direct ink writing. This approach employs multi-material extrusion for the production of structures with passive and active features, rapid device fabrication, and improved design freedom. A model of the thermal doping and extrusion processes is proposed that enables designers to predict the extruded track width and tune process parameters as required. These processes have been applied to the fabrication of both standalone polyaniline-based 3D structures and embedded strain sensors capitalizing on the piezoresistive properties of polyaniline.

Keywords: conjugated polymers, additive manufacturing, polyaniline, direct ink writing, fused filament fabrication, conductive electroactive polymers, piezoresistivity.

There are many branches of manufacturing industry which greatly depend for their success upon the designer's art, and it is necessary that the industrial designer should possess a knowledge of the processes of the manufacture in which his designs will be utilized, as well as of the properties and capabilities of the material to which they will be applied.

– Sir Philip Magnus

Industrial education, K. Paul,

Trench & Co., 1888. pp. 24–25

Dedication

Dedicated to my parents.

Acknowledgements

Financial support for my studies was generously provided by NSERC Canada through Discovery Grant RGPIN-2015-05014 "Toward 3D Printing Technologies for the Fabrication of Nanoscale Actuator Arrays", SPIE Student Author Travel Grant, Western Society of Graduate Students Travel Subsidy, and the University of Western Ontario.

Thanks to my Program Advisor, Prof. Robert Klassen for his support and guidance throughout the project. Thanks to the members of the Micro-Nano-Bio Systems Lab for their time and effort in providing access and training for essential characterization equipment. Thanks to Alicia Robinet for her writing support and editing services. Thanks also to Undergraduate Research Assistant Robert Meagher, for providing valuable programming assistance.

Special thanks to my supervisor Prof. Aaron Price for his continual support, generosity with his time and advice, and for his commitment to the dissemination of work providing the opportunity to connect with researchers at the forefront of the field at international conferences. Your dedication to research, education, and family is an inspiration.

Thank you to my colleagues in the Organic Mechatronics and Smart Materials Laboratory, especially Andrew Cullen, for your camaraderie in handling the rigours of graduate studies. Finally, thanks to my dearest friends and family. I owe special gratitude to my parents for instilling in me their tireless work ethic, and for their unrelenting support to ensure I had everything I needed to pursue my goals.

I am forever grateful for your friendship, guidance, and support. Thank you all.

Contents

Contents vi

List of Tables ix

List of Figures x

List of Acronyms and Symbols xii

1 Introduction 1

1.1 Objectives 2

1.2 Major contributions 3

1.3 Organization of the thesis 4

List of references 5

2 Background 7

2.1 Conjugated polymers 7

2.1.1 Background 7

2.1.2 Synthesis of PANI for improving processability 10

2.1.3 Counterion-induced thermal doping 12

2.2 Additive manufacturing 14

2.3 Chapter summary 15

List of references 16

3 PANI-DBSA paste preparation and characterization 21

3.1 Polyaniline synthesis 21

3.2 PANI-DBSA paste preparation 25

3.3 PANI-DBSA paste characterization 26

3.3.1 Methodology 26

3.3.2 Results and discussion 27

3.4 Chapter summary 29

List of references 31

4 Direct ink writing apparatus development and process modelling 33

4.1 Apparatus development 34

4.1.1 Fused filament fabrication delta robot 34

4.1.2 General AM process 35

4.1.3 Initial paste extrusion system 36

4.1.4 Final paste extrusion system 39

4.1.5 G-code preparation and modification 41

4.2 PANI-DBSA extruded track width study 42

4.2.1 Model development 42

4.2.2 Methods 43

4.2.3 Results and discussion 44

4.3 Sample 3D PANI-based structures 46

4.4 Chapter summary 49

List of references 51

5 Application of PANI in embedded strain sensor 52

5.1 Introduction 52

5.2 Methods 53

5.2.1 Sensor fabrication procedure 53

5.2.2 Post-extrusion thermal doping 54
5.2.3 Sensor performance characterization 55
5.3 Results and discussion 56
5.4 Chapter summary 61
List of references 62

6 Concluding remarks **63**
6.1 Summary of conclusions 63
6.2 Summary of contributions 64
6.3 Recommendations for future research 65

Appendices **67**

A Software code listing **68**
A.1 Steps per mm converter python script 68
A.2 Stepper motor to Ultimus V signal conversion 69

B Curriculum Vitae **70**

List of Tables

3.1 Polyaniline material cost by source 24

List of Figures

2.1 Breakdown of CP research published from 1990–2000 9
2.2 Chemical structures of a fundamental group conjugated polymers 10
2.3 Conductivity comparison of various CP and common conductors 11
2.4 Doping process converting EB to conductive ES 11
2.5 Temperature change of PANI-DBSA during counterion-induced thermal doping 13
2.6 Formation of layered structure in PANI-DBSA complex 13
2.7 Comparison of additive and subtractive manufacturing methods 14
2.8 Comparison of FFF and DIW methods 16

3.1 Schematic of PANI polymerization procedure 22
3.2 Shear thinning results for different thermal doping times 29
3.3 Graph showing power law constants as a function of heating time 30

4.1 Standard configuration of delta 3D printer 35
4.2 DM and paste extruder 38
4.3 Final printed part and LED test 39
4.4 Schematic of direct ink writing fabrication apparatus 41
4.5 Track width image processing 44
4.6 Track width model validation 47
4.7 Variation in extruded tracks 48

4.8 Dimensional errors in extruded tracks 48
4.9 3D PANI-DBSA structures 50

5.1 Embedded PANI strain sensor fabrication 54
5.2 Strain sensor characterization stretching apparatus 57
5.3 Resistance response of first 2 stretching cycles 58
5.4 Combined Stability Results 59
5.5 GF results 60
5.6 Delamination of PANI-DBSA from support material 61

List of Acronyms and Symbols

Acronyms

2D	2-dimensional
3D	3-dimensional
ABS	acrylonitrile butadiene styrene
AM	additive manufacturing
APS	ammonium persulfate
ASTM	American Section of the International Association for Testing Materials
CAD	computer-aided design
CITD	counterion-induced thermal doping
CNC	computer numerical control
CP	conjugated polymer
CSA	camphorsulfonic acid
DBSA	dodecylbenzenesulfonic acid
DC	direct current
DIW	direct ink writing
EAP	electroactive polymer
EB	emeraldine base
ES	emeraldine salt
FFF	fused filament fabrication
GF	gauge factor

IUAPAC	International Union of Pure and Applied Chemistry
LED	light-emitting diode
PA	polyacetylene
PANI	polyaniline
PMMA	poly(methyl methacrylate)
PPy	polypyrrole
PS	polystyrene
PVC	polyvinyl chloride
STL	stereolithography file format
TPE	thermoplastic elastomer

Greek symbols

ε	mechanical strain
η	apparent viscosity
η_0	consistency constant
$\dot{\gamma}$	shear rate
ν	Poisson's ratio
ρ	resistivity

Latin symbols

D	nozzle diameter
d	extruded track width
ΔP	gauge pressure
L	nozzle length
l	strain sensor length
n	power law index
R	electrical resistance
r	coefficient of correlation
r^2	coefficient of determination

t_{doping}	thermal doping time
v	end effector travel speed

Chapter 1

Introduction

The sensing and actuation capabilities of electroactive polymers (EAP) in response to electrical stimuli have attracted significant research interest (Bar-Cohen, 2004). One class of electroactive polymer of particular interest in the research community are the conjugated polymers (CP) (Blythe, 1984). CP are organic polymers characterized by their conjugated backbone structure that enables electrical conductivity via charge delocalization. This combination of the electrical properties of semiconductors and the mechanical properties of polymers has led to application of CP in batteries, electrochromic devices, corrosion barriers, anti-static films, sensors and artificial muscle actuators (Wallace et al., 2009; Castillo-Ortega et al., 2003). The polymer polyaniline (PANI) is one highly studied CP that exhibits environmental stability, biocompatibility, and ease of synthesis while maintaining a relatively low cost of synthesis (Adams et al., 1994; Kamalesh et al., 2000). However, the unique structure of these materials that allow for conductivity also greatly reduces their processability resulting in conventional polymer processing techniques being unsuitable. The intractable nature of CP has limited advances in fabrication techniques to 2D film deposition methods. While there have been significant advances in 2D film deposition techniques the fabrication of complex 3D structures for more advanced sensing applications has yet to be ex-

plored (Yoshioka and Jabbour, 2006; Ung et al., 2013).

One barrier to the widespread application of PANI is associated with its inability to be conventionally melt-processed due to degradation in material properties before the glass transition temperature being reached (Cao et al., 1992; Laska et al., 1995; Wang et al., 1995). To achieve the required processability of PANI a counter-ion induced thermal doping method has been employed. In this method, PANI is combined with a protonic acid having a functional group large enough to disrupt the interchain bonding in the PANI resulting in the formation of a viscous paste. Typically, this method has been used in the formation of conductive composite materials by enabling PANI to be processed with a bulk polymer such as poly(vinyl chloride) (PVC) (Proń et al., 1993). However, with further understanding of this thermal doping process it has been adapted to obtain PANI-based pastes formulated for extrusion based additive manufacturing (AM) methods. Through integration of conventional AM techniques and development of a multi-material robotic paste extrusion system the rapid development of high-resolution conductive 3D PANI structures may be realized, free of previous limitations.

1.1 Objectives

This project aims to develop a novel additive manufacturing method specifically tailored for the fabrication of complex 3D conductive structures of PANI for actuators and transducers. To achieve this goal, the following research objectives are proposed:

- *Develop synthesis method of PANI and paste preparation process optimized for extrusion based additive manufacturing.* The first objective is to develop a synthesis method of PANI that will allow control over the properties of the polymer and provides a lower cost supply of materials for process development. A treatment method will be developed to enable the production of PANI-based pastes specially formulated for extrusion methods and investigate impact of mixing process

parameters to tune the properties of the paste. Finally, characterization of the flow properties of the paste based on mixing process parameters will be performed.

- *Develop fabrication apparatus for production of PANI-based devices and modelling to predict extruded track width.* The second objective is to develop a fabrication apparatus for the production of high-resolution 3D structures that can be applied to sensors and actuators. This system should also maintain the functionality of a conventional FFF 3D printer to allow for concurrent deposition of thermoplastics and paste-based materials. Additionally, a model should be proposed that incorporates the variation of key process parameters to predict the extruded track width. This will allow any designer to implement the process with a basic understanding of the process while still capitalizing on the unique potential of the system.

- *Demonstrate the novel application of 3D conductive PANI transducers fabricated by additive manufacturing techniques.* The third objective is to demonstrate the use of this novel fabrication system for the direct production of functional PANI devices. This device should contain passive and active structures created concurrently and capitalize on the unique potential of the fabrication system and the properties of PANI.

1.2 Major contributions

This thesis conveys the following major contributions to the scientific body of knowledge:

- *Novel PANI paste preparation method formulated for additive manufacturing.* The first-ever study of the counter-ion thermal doping method of PANI for the application of additive manufacturing. This has been achieved through the characteri-

zation of the relationship between thermal doping time and paste flow properties with a focus on apparent viscosity.

- *Multi-material direct ink writing extrusion system.* Integrated a conventional fused filament fabrication delta robot with a paste extrusion system to enable the concurrent deposition of fluid based materials and conventional additive manufacturing filament based materials. This apparatus not only allows for the fabrication of complex, high-resolution 3D conductive PANI structures but also the introduction of passive and active features with the ability to embed active materials in a passive support structure.

- *Modelling of PANI direct ink writing extrusion process.* Adaptation of model for the direct ink writing of bioinks to the applications of PANI-based paste extrusion has been explored. This model incorporates key process parameters and material properties to allow a user to design the fabrication process with application specific parameters. The model predicts the extruded track width based upon material flow properties and process parameters such as print speed, nozzle diameter, and extrusion pressure.

- *Embedded PANI piezoresistive strain sensor.* The first ever example of the in-situ embedding of a PANI-based sensor through AM techniques. This sensor capitalizes on the piezoresistive property of PANI and embedded in a flexible TPE support material to create a compliant sensor.

1.3 Organization of the thesis

The following chapter, Chapter 2, *Background* summarizes the fundamental knowledge in CP structure, properties, and applications. Following discussion of the benefits and associated limitations of PANI, a brief introduction is provided in AM techniques and

how they may be adapted for fabrication of conductive polymer devices. In accordance with the aforementioned objectives, the remainder of the thesis is organized as follows: Chapter 3, *PANI-DBSA paste preparation and characterization* explores the development of PANI-based pastes specially formulated for AM and their rheological characterization as a function of processing parameters. Next, Chapter 4, *Direct ink writing apparatus development and process modelling* explores the integration of a conventional FFF delta robot with a paste extrusion system to combine the resolution and design freedom of AM techniques to develop a multi-material extrusion CNC delta robot. This chapter also introduces the modelling and validation of the PANI paste extrusion process. Chapter 5, *Application of PANI in embedded strain sensor* provides a study on the practical engineering application of an embedded PANI-based piezoelectric strain sensor. Finally, Chapter 6, *Concluding remarks* summarizes the primary conclusions of the work, recapitulates the main contributions to knowledge, and provides recommendations for future research.

List of references

Adams, P. N., Laughlin, P. J., Monkman, A. P. and Bernhoeft, N. (1994), 'A further step towards stable organic metals. Oriented films of polyaniline with high electrical conductivity and anisotropy', *Solid State Communications* **91**(11), 875–878.

Bar-Cohen, Y., ed. (2004), *Electroactive Polymer (EAP) Actuators as Artificial Muscles: Reality, Potential, and Challenges*, 2nd edn, SPIE Press, Bellingham, WA.

Blythe, A. (1984), 'Electrical resistivity measurements of polymer materials', *Polymer Testing* **4**(2–4), 195–209.

Cao, Y., Smith, P. and Heeger, A. J. (1992), 'Counter-ion induced processibility of con-

ducting polyaniline and of conducting polyblends of polyaniline in bulk polymers', *Synthetic Metals* **48**(1), 91–97.

Castillo-Ortega, M. M., Del Castillo-Castro, T., Encinas, J. C., Perez-Tello, M., De Paoli, M. and Olayo, R. (2003), 'Electrically conducting polyaniline-PBMA composite films obtained by extrusion', *Journal of Applied Polymer Science* **89**(1), 179–183.

Kamalesh, S., Tan, P., Wang, J., Lee, T., Kang, E. T. and Wang, C. H. (2000), 'Biocompatibility of electroactive polymers in tissues', *Journal of Biomedical Materials Research* **52**(3), 467–478.

Laska, J., Pron, A., Zagorska, M., Łapkowski, S. and Lefrant, S. (1995), 'Thermally processable conducting polyaniline', *Synthetic Metals* **69**(1-3), 113–115.

Proń, A., Laska, J., Österholm, J.-E. and Smith, P. (1993), 'Processable conducting polymers obtained via protonation of polyaniline with phosphoric acid esters', *Polymer* **34**(20), 4235–4240.

Ung, B. S.-Y., Weng, B., Shepherd, R., Abbott, D. and Fumeaux, C. (2013), 'Inkjet printed conductive polymer-based beam-splitters for terahertz applications', *Optical Materials Express* **3**(9), 1242.

Wallace, G. G., Spinks, G. M., Kane-Maguire, L. A. and Teasdale, P. R. (2009), *Conductive Electroactive Polymers: Intelligent Polymer Systems*, 3rd edn, CRC Press, Boca Raton, FL.

Wang, X.-H., Geng, Y.-H., Wang, L.-X., Jing, X.-B. and Wang, F.-S. (1995), 'Thermal behaviors of doped polyaniline', *Synthetic Metals* **69**(1-3), 265–266.

Yoshioka, Y. and Jabbour, G. E. (2006), 'Desktop inkjet printer as a tool to print conducting polymers', *Synthetic Metals* **156**(11–13), 779–783.

Chapter 2

Background

This chapter provides background information regarding fundamental research into CP, specifically PANI, and highlights the unique properties of these materials that can be exploited for the fabrication of transducers and other applications. Synthesis routes for improving the processability of PANI are presented with a focus on counterion-induced thermal doping. AM techniques are presented as a method to overcome the current limitations in the fabrication of 3D PANI structures. The conventional additive methods of fused filament fabrication and direct ink writing are presented as the recommended methods to realize PANI-based transducers.

2.1 Conjugated polymers

2.1.1 Background

Research interest in conjugated polymers was initiated by the work of Shirakawa, MacDiarmid, and Heeger in the development of polyacetylene (PA) for which they were later awarded the Nobel Prize for this work (Shirakawa et al., 1977). Their work with PA led to the discovery and development of a number of other CP including: polypyrrole (PPy), polythiophene, poly(p-phenylene), and PANI. Conjugated polymers are intrinsically con-

ductive based upon the nature of their polymer backbone structure, Figure 2.2. This conjugated structure is composed of alternating single and double bonds along the polymer chain. This new class of materials led to exciting research in the pursuit of capitalizing the electrical properties of conductors and semiconductors with the mechanical properties of polymers. This research has focused largely on fundamental properties of the materials towards improving their synthesis and conductivity, whereas research towards applications accounts for approximately 20% of publications, Figure 2.1 (Wallace et al., 2009). CP have been applied in energy storage applications as electrode materials, corrosion protection, anti-static films, actuators, and sensors (Genies et al., 1990; Wang et al., 2002; Crowley et al., 2008; Ćirić-Marjanović, 2013). However, the structure that renders these materials conductive also results in poor stability and solubility resulting in limitations to processability. PA exhibits conductivity near copper but has very poor environmental stability making practical application challenging, Figure 2.3 (Bhadra et al., 2009). This trade off between material properties, stability and processability exists throughout the group of CP. PANI has been a widely studied CP because it exhibits a balance between this issues, demonstrating sufficient conductivity, processability, superior environmental stability and biocompatibility while maintain a low cost of production (Adams et al., 1994; Kamalesh et al., 2000).

As previously stated, the chemical structure of CP enables their conductivity. While the underlying physics explaining this process are beyond the scope of this work, it is important to understand factors that can impact their conductivity. In the case of PANI, it can undergo redox reactions allowing it to exist at 6 oxidation states, where the degree of protonation of the polymer chain directly effects conductivity. One of the key contributors to conductivity is the oxidation level and molecular arrangement (MacDiarmid et al., 1987). The three main oxidation states are: fully reduced leucoemeraldine, fully oxidized pernigraniline, and half oxidized/reduced emeraldine. Additionally, each of these states can be modified by a process called *doping* through the addition of protons to the

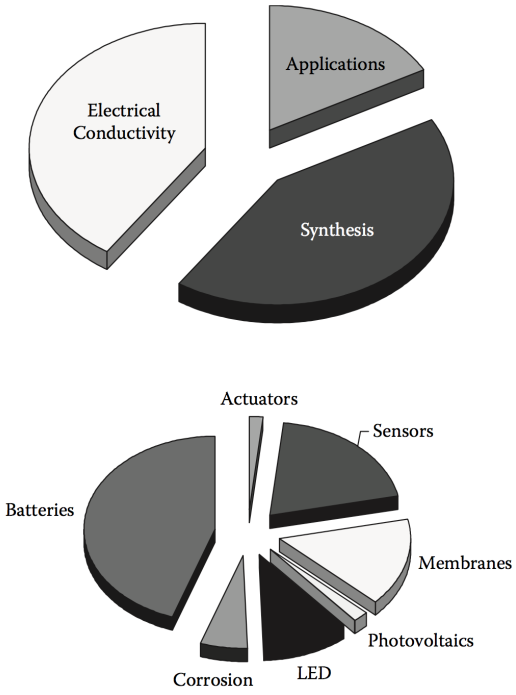

Figure 2.1: The distribution of CP research published (1990–2000) shows a focus on synthesis and properties of the material, applications such as energy storage and transducers have also been investigated but not as widely (© Wallace et al., 2009, included with permission).

structure, the insulating base form can be converted to a doped salt state, Figure 2.4. The only oxidation state that exhibits conductive behaviour is emeraldine salt (ES). This is because the conductivity of PANI is provided by the formation of polaron structures, which can only be formed in this molecular arrangement, in this structure delocalization of charge is achieved. MacDiarmid and Epstein (1995) and Avlyanov et al. (1995) have determined that this secondary acid doping can have great impact on the electrical and mechanical properties as well as the processability of PANI and can be used to develop solution processable formulations. Other factors affecting the conductivity of PANI, to a lesser degree, are molecular weight; due to the bulk conductivity being a function of inter- and intra-molecular conductivity, percentage crystallinity and inter-chain separation, while the two main factors remain the oxidation state, type of dopant, and degree of doping (Stejskal et al., 1998; Cao et al., 1989).

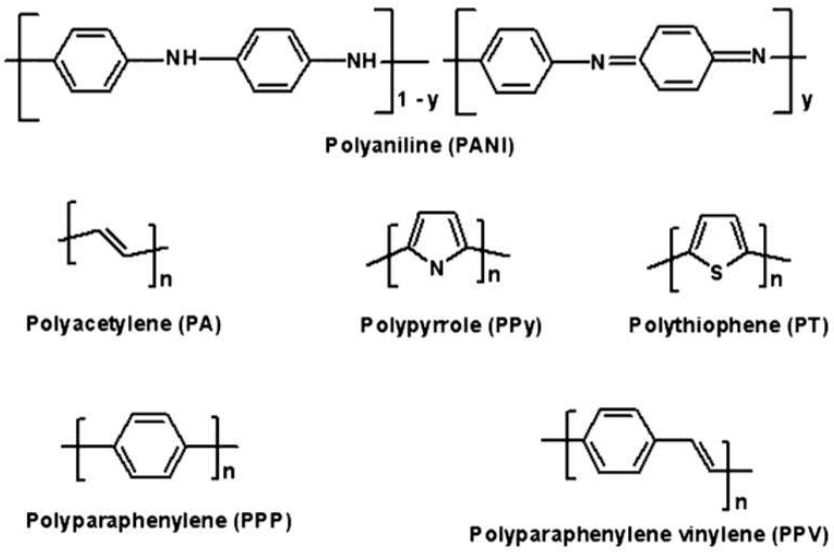

Figure 2.2: The chemical structures of a fundamental group of conjugated polymers (© Bhadra et al., 2009, included with permission).

2.1.2 Synthesis of PANI for improving processability

One issue with the ES oxidation state is its poor processability due to a large degree of hydrogen bonding rendering it generally intractable, as such, it cannot be processed by conventional techniques (Heeger, 1993). One of the main areas of research for PANI has been the development of conductive composites, this trend is built around the elimination of the need for conductive fillers like carbon black and carbon nanotubes (Bhattacharya and De, 1999; Ruiz et al., 2012). Part of the requirement for these techniques is the ability to commercialize the process, therefore they must be scalable and inexpensive. The two main routes pursued have been synthetic methods and blending methods (Anand et al., 1998). In synthetic methods, the focus is typically the direct polymerization of one or both of a matrix polymer and aniline to obtain a composite. In blending methods, typically the composite constituents are combined in solution after treatment of PANI to achieve the required solubility. From the blending methods came the discovery of counterion-induced processability. Cao et al. (1992) showed that doping EB with functionalized protonic acids, dodecylbenzenesulfonic acid (DBSA) and

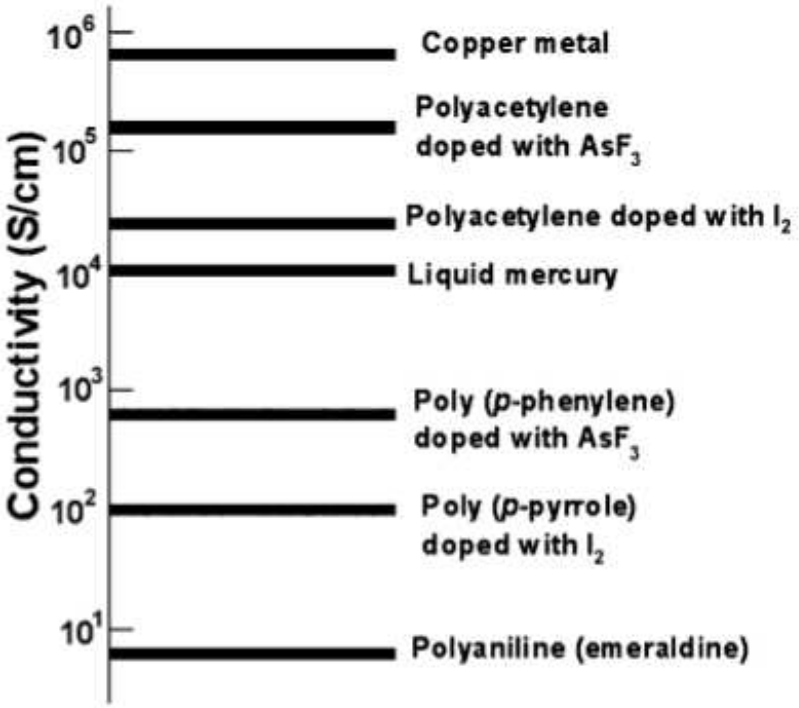

Figure 2.3: Comparing the conductivities of some CP and common conductors shows the wide range within the group of CP (© Bhadra et al., 2009, included with permission).

camphorsulfonic acid (CSA) for example, of the form, $H^+(M^-R)$ where H^+M^- is the acid group and R is an organic group, that the solubility of PANI in common solvents could be achieved. This method was leveraged to solution process PANI to create composites with matrix polymers of PC, PMMA, Nylon, polyvinylacetate, and ABS (Haba et al., 2000; Pud, 2003). Ongoing research towards improving the processability of PANI has focused on solution-based techniques and has not lead to significant development of the foundational work in counterion-induced thermal doping (Jaymand,

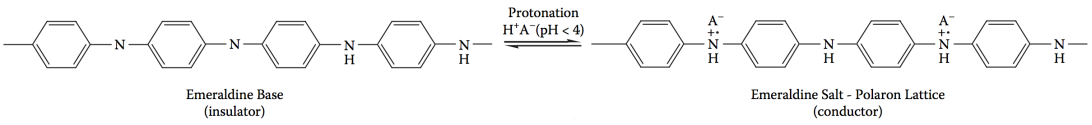

Figure 2.4: The reversible redox doping reaction to convert from insulating EB to conductive ES oxidation state through protonation/deprotonation of the polymer chain (© Wallace et al., 2009, included with permission).

2013).

2.1.3 Counterion-induced thermal doping

The discovery of the improved solution processability of PANI was further developed by Levon et al. (1995), who introduced the concept of a method to dope PANI with DBSA without the use of an auxiliary solvent. This was achieved through counterion-induced thermal doping, where chemical complexation is achieved by combining the constituents with applied heat. Heat is a key requirement in this process because near room temperature there is strong self-association of DBSA and PANI causing slow diffusion rates. With the addition of heat there is sufficient energy to accelerate the diffusion process and overcome these self-association forces. The seminal work by Titelman et al. (1997), outlines the stages of the thermal doping process and are shown in Figure 2.5. Before heating, PANI particles are coated in DBSA creating core-shell structure, and under heated mixing the temperature increases above the initial heating temperature and the paste transitions to a semi-solid stage, and may undergo some swelling effects (Ahlskog et al., 1995). At this point the exothermic doping reaction is almost fully complete and additional heat generation is attributed to frictional effects presented by the mixing apparatus. Optimal mixing temperatures have been reported to initiate thermal doping to completion without degrading material properties. Titelman et al. (1997) determined that the optimal initial mixing temperature is 143 °C and at temperatures below 132 °C the reaction was incomplete and full doping was not achieved. Additionally, Levon et al. (1995) and Zilberman et al. (1997) reported that material degradation is initiated at 175 °C. Lastly, the exothermic peaks for these reactions typically occurred between $5 - 15$ min of mixing time.

The use of a functionalized protonic acid improves the processability of PANI in its conductive state by disrupting interchain bond and lowering the glass transition temperature. However, another interesting phenomena was seen by Levon et al. (1995),

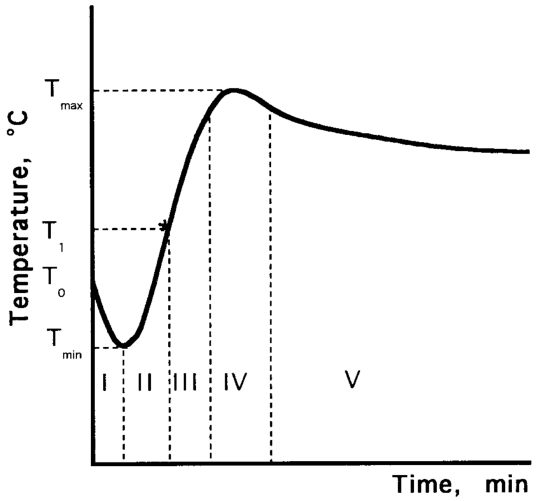

Figure 2.5: The temperature profile of PANI-DBSA during counterion-induced thermal doping changes dramatically due to the exothermal complexation of the constituents (© Titelman et al., 1997, included with permission).

where the alkyl side chains created separation in the polymer chains and prevented the formation of close packing. This results in an anisotropic, layered structure that may be exploited in the processing or final application.

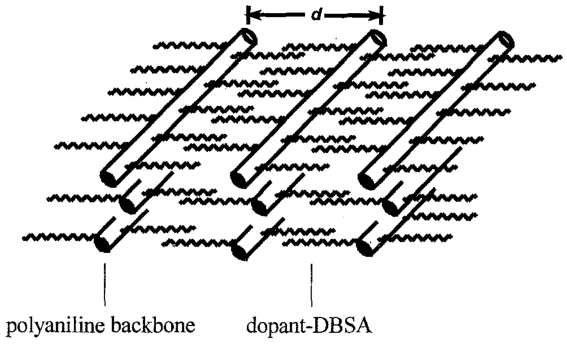

Figure 2.6: Representation of the layered structure in PANI-DBSA complex formed during counterion-induced thermal doping (© Levon et al., 1995, included with permission).

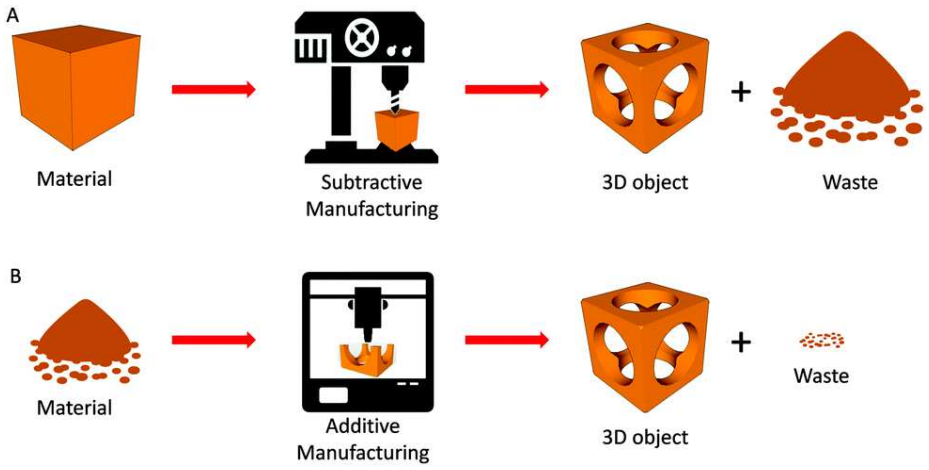

Figure 2.7: Comparison of additive and subtractive manufacturing methods. (A) Subtractive methods consist of removing material from a workpiece. (B) In additive manufacturing there is controlled processing and deposition of material to build the structure (© Ambrosi and Pumera, 2016, included with permission).

2.2 Additive manufacturing

Additive Manufacturing (AM), commonly known as 3D printing, refers to the process of joining materials to make parts from 3D model data, usually through the formation of successive layers, as opposed to subtractive and formative manufacturing methods (ASTM Standard F2792-12A, 2012). A fundamental difference between AM and subtractive methods is the reduction in waste by eliminating a sacrificial work piece and only depositing material in the required locations to manufacture the part, Figure 2.7. AM can be used to simplify the manufacturing process by reducing the complexity of the system, tool changes required, or even process changes. AM can be classified into 4 main groups based upon the mechanism for layer deposition or adhesion: photopolymerization, powder based, lamination, and finally extrusion (Ambrosi and Pumera, 2016).

This review will focus on extrusion-based techniques with the aim of combining counterion-induced thermal doping approaches and AM techniques for the fabrication of PANI-based devices. Extrusion-based methods are amongst the mostly widely used

AM techniques, these methods involve the deposition of material from a nozzle located on a controllable printhead (Turner and Gold, 2015). The two types of AM that employ extrusion are fused filament fabrication (FFF) or fused deposition modelling, and direct ink writing (DIW) which is also referred to as robocasting (Lewis et al., 2006). The key difference between these techniques is that FFF uses a heated printhead to melt and extrude thermoplastic materials and the shape of the final part is achieved by cooling of extruded filament allowing successive layers to be deposited on it, Figure 2.8A (Turner et al., 2014). Whereas in DIW, a fluid-based material is forced through a nozzle and undergoes a curing or drying process to maintain its extruded geometry. There are a wide range of materials used in DIW including: colloidal inks, ceramic slurries, hydrogels, bio-inks, and polymeric melts, Figure 2.8B (Lewis, 2006). These materials have been applied to tissue engineering scaffolds, microfluidic devices, batteries, and sensors (Lewis, 2006; Kang et al., 2016). Material design is essential for the ability to create high-resolution features and can be tuned for the application. For effective ink design the extruded material must be able to span gaps, creating bridges, and produce high aspect-ratio features, while also avoiding unwanted voids between adjacent extruded tracks. Further aspects of the AM techniques employed in this research are discussed in greater detail in Chapter 4, *Direct ink writing apparatus development and process modelling*, including: configuration, software, model preparation, and relevant process parameters.

2.3 Chapter summary

This chapter provided the background information and framework for the research conducted in this thesis. The unique properties of CP have lead to research into the improvement of their processability to achieve a wider range of applications, however, methods to realize 3D PANI structures are limited. Synthesis routes for processable

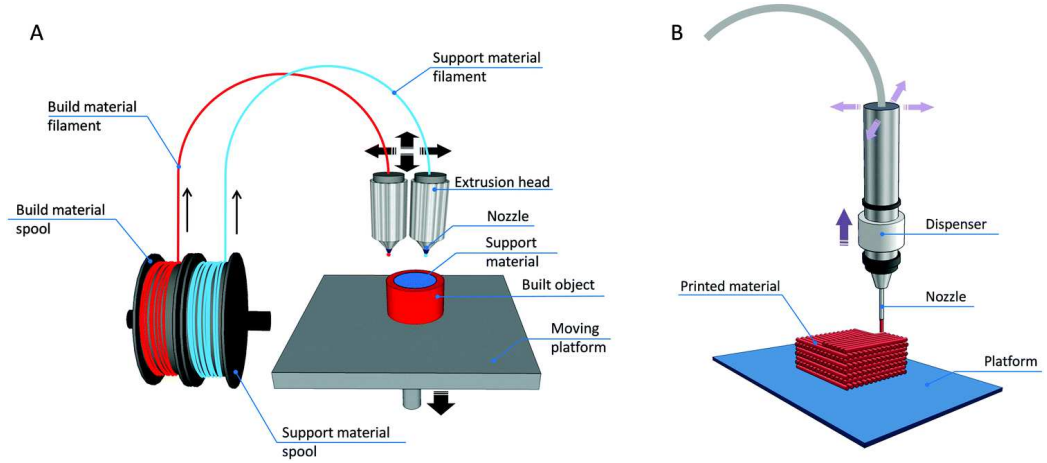

Figure 2.8: Schematics of FFF and DIW methods. (A) In FFF a thermoplastic filament is fed through a heated nozzle to deposit a track of molten material which rapidly welds to the previous layer. (B) In DIW a fluid-based material is forced through the nozzle in a similar manner to create a layered structure which can be cured to finalize the geometry (© Ambrosi and Pumera, 2016, included with permission).

PANI include counterion-induced thermal doping whereby through the heated mixing of PANI with DBSA a viscous paste can be formed creating the potential for extrusion via DIW. AM techniques were outlined and the methods of FFF and direct ink writing were discussed as a methods towards the first realization of PANI-based transducers consisting of high-resolution, 3D, and conductive structures.

List of references

Adams, P. N., Laughlin, P. J., Monkman, A. P. and Bernhoeft, N. (1994), 'A further step towards stable organic metals. Oriented films of polyaniline with high electrical conductivity and anisotropy', *Solid State Communications* **91**(11), 875–878.

Ahlskog, M., Isotalo, H., Ikkala, O., Laakso, J., Stubb, H. and Österholm, J.-E. (1995), 'Heat-induced transition to the conducting state in polyaniline/dodecylbenzenesulfonic acid complex', *Synthetic Metals* **69**(1-3), 213–214.

Ambrosi, A. and Pumera, M. (2016), '3D-printing technologies for electrochemical applications.', *Chemical Society Reviews* **45**(10), 2740–2755.

Anand, J., Palaniappan, S. and Sathyanarayana, D. N. (1998), 'Conducting polyaniline blends and composites', *Progress in Polymer Science* **23**(6), 993–1018.

ASTM Standard F2792-12A (2012), *Terminology for Additive Manufacturing Technologies*, ASTM International, West Conshohocken, PA.

Avlyanov, J. K., Min, Y., MacDiarmid, A. G. and Epstein, A. J. (1995), 'Polyaniline: conformational changes induced in solution by variation of solvent and doping level', *Synthetic Metals* **72**(1), 65–71.

Bhadra, S., Khastgir, D., Singha, N. K. and Lee, J. H. (2009), 'Progress in preparation, processing and applications of polyaniline', *Progress in Polymer Science* **34**(8), 783–810.

Bhattacharya, A. and De, A. (1999), 'Conducting polymers in solution - Progress toward processibility', *Journal of Macromolecular Science-Reviews in Macromolecular Chemistry and Physics* **C39**(1), 17–56.

Cao, Y., Andreatta, A., Heeger, A. J. and Smith, P. (1989), 'Influence of chemical polymerization conditions on the properties of polyaniline', *Polymer* **30**(12), 2305–2311.

Cao, Y., Smith, P. and Heeger, A. J. (1992), 'Counter-ion induced processibility of conducting polyaniline and of conducting polyblends of polyaniline in bulk polymers', *Synthetic Metals* **48**(1), 91–97.

Ćirić-Marjanović, G. (2013), 'Recent advances in polyaniline research: Polymerization mechanisms, structural aspects, properties and applications', *Synthetic Metals* **177**, 1–47.

Crowley, K., O'Malley, E., Morrin, A., Smyth, M. R. and Killard, A. J. (2008), 'An aqueous ammonia sensor based on an inkjet-printed polyaniline nanoparticle-modified electrode.', *The Analyst* **133**(3), 391–399.

Genies, E. M., Boyle, A., Lapkowski, M. and Tsintavis, C. (1990), 'Polyaniline - a Historical Survey', *Synthetic Metals* **36**(2), 139–182.

Haba, Y., Segal, E., Narkis, M., Titelman, G. I. and Siegmann, a. (2000), 'Polyaniline-DBSA/polymer blends prepared via aqueous dispersions', *Synthetic Metals* **110**(3), 189–193.

Heeger, A. J. (1993), 'Polyaniline with surfactant counterions: conducting polymer materials which are processible in the conducting form', *Synthetic Metals* **57**(1), 3471–3482.

Jaymand, M. (2013), 'Recent progress in chemical modification of polyaniline Dedicated to Professor Dr. Ali Akbar Entezami.', *Progress in Polymer Science* **38**(9), 1287–1306.

Kamalesh, S., Tan, P., Wang, J., Lee, T., Kang, E. T. and Wang, C. H. (2000), 'Biocompatibility of electroactive polymers in tissues', *Journal of Biomedical Materials Research* **52**(3), 467–478.

Kang, H.-W., Lee, S. J., Ko, I. K., Kengla, C., Yoo, J. J. and Atala, A. (2016), 'A 3D bioprinting system to produce human-scale tissue constructs with structural integrity', *Nature Biotechnology* **34**(3), 312.

Levon, K., Ho, K.-H., Zheng, W.-Y., Laakso, J., Kärnä, T. and Österholm, J.-E. (1995), 'Thermal doping of polyaniline with dodecylbenzene sulfonic acid without auxilary solvents', *Polymer* **36**(14), 2733–2738.

Lewis, J. A. (2006), 'Direct Ink Writing of 3D Functional Materials', *Advanced Functional Materials* **16**(17), 2193–2204.

Lewis, J. A., Smay, J. E., Stuecker, J. and Cesarano, J. (2006), 'Direct Ink Writing of Three-Dimensional Ceramic Structures', *Journal of the American Ceramic Society* **89**(12), 3599–3609.

MacDiarmid, A., Chiang, J., Richter, A. and Epstein, A. (1987), 'Polyaniline: a new concept in conducting polymers', *Synthetic Metals* **18**(1), 285 – 290. Proceedings of the International Conference of Science and Technology of Synthetic Metals.

MacDiarmid, A. G. and Epstein, A. J. (1995), 'Secondary doping in polyaniline', *Synthetic Metals* **69**(1-3), 85–92.

Pud, A. (2003), 'Some aspects of preparation methods and properties of polyaniline blends and composites with organic polymers', *Progress in Polymer Science (Oxford)* **28**(12), 1701–1753.

Ruiz, J., Gonzalo, B., Dios, J. R., Laza, J. M., Vilas, J. L. and León, L. M. (2012), 'Improving the Processability of Conductive Polymers: The Case of Polyaniline', *Advances in Polymer Technology* **32**(S1), E180–E188.

Shirakawa, H., Louis, E. J., MacDiarmid, A. G., Chiang, C. K. and Heeger, A. J. (1977), 'Synthesis of electrically conducting organic polymers: halogen derivatives of polyacetylene, $(CH)_x$', *Journal of the Chemical Society, Chemical Communications* (16), 578–3.

Stejskal, J., Riede, A., Hlavatá, D., Prokeš, J., Helmstedt, M. and Holler, P. (1998), 'The effect of polymerization temperature on molecular weight, crystallinity, and electrical conductivity of polyaniline', *Synthetic Metals* **96**(1), 55–61.

Titelman, G. I., Zilberman, M., Siegmann, A., Haba, Y. and Narkis, M. (1997), 'Thermal dynamic processing of polyaniline with dodecylbenzene sulfonic acid', *Journal of Applied Polymer Science* **66**(12), 2199–2208.

Turner, B. N. and Gold, S. A. (2015), 'A review of melt extrusion additive manufacturing processes: II. Materials, dimensional accuracy, and surface roughness', *Rapid Prototyping Journal* **21**(3), 250–261.

Turner, B. N., Strong, R. and Gold, S. A. (2014), 'A review of melt extrusion additive manufacturing processes: I. Process design and modeling', *Rapid Prototyping Journal* **20**(3), 192–204.

Wallace, G. G., Spinks, G. M., Kane-Maguire, L. A. and Teasdale, P. R. (2009), *Conductive Electroactive Polymers: Intelligent Polymer Systems*, 3rd edn, CRC Press, Boca Raton, FL.

Wang, H.-L., Gao, J., Sansiñena, J. M. and McCarthy, P. (2002), 'Fabrication and characterization of polyaniline monolithic actuators based on a novel configuration: Integrally skinned asymmetric membrane', *Chemistry of Materials* **14**(6), 2546–2552.

Zilberman, M., Titelman, G. I., Siegmann, A., Haba, Y., Narkis, M. and Alperstein, D. (1997), 'Conductive blends of thermally dodecylbenzene sulfonic acid-doped polyaniline with thermoplastic polymers', *Journal of Applied Polymer Science* **66**(2), 243–253.

Chapter 3

Development and rheological modelling of PANI-DBSA paste via counterion-induced thermal doping

This chapter outlines the development of a PANI-based paste specially formulated for DIW. A chemical oxidative synthesis route is outlined to maintain control over the properties of PANI used in paste preparation and greatly reduce the material cost. The application of counterion-induced thermal doping to develop a process to produce PANI-DBSA is presented. This process involves mixing of paste constituents while heating. The characterization of the rheological behaviour of the material based on the processing parameters is investigated. Finally, an empirical model relating the length of thermal doping time to the flow behaviour of the resultant paste is proposed.

3.1 Polyaniline synthesis

PANI is commonly synthesized via chemical oxidative polymerization or electrochemical polymerization (Wallace et al., 2009). Chemical oxidative polymerization was em-

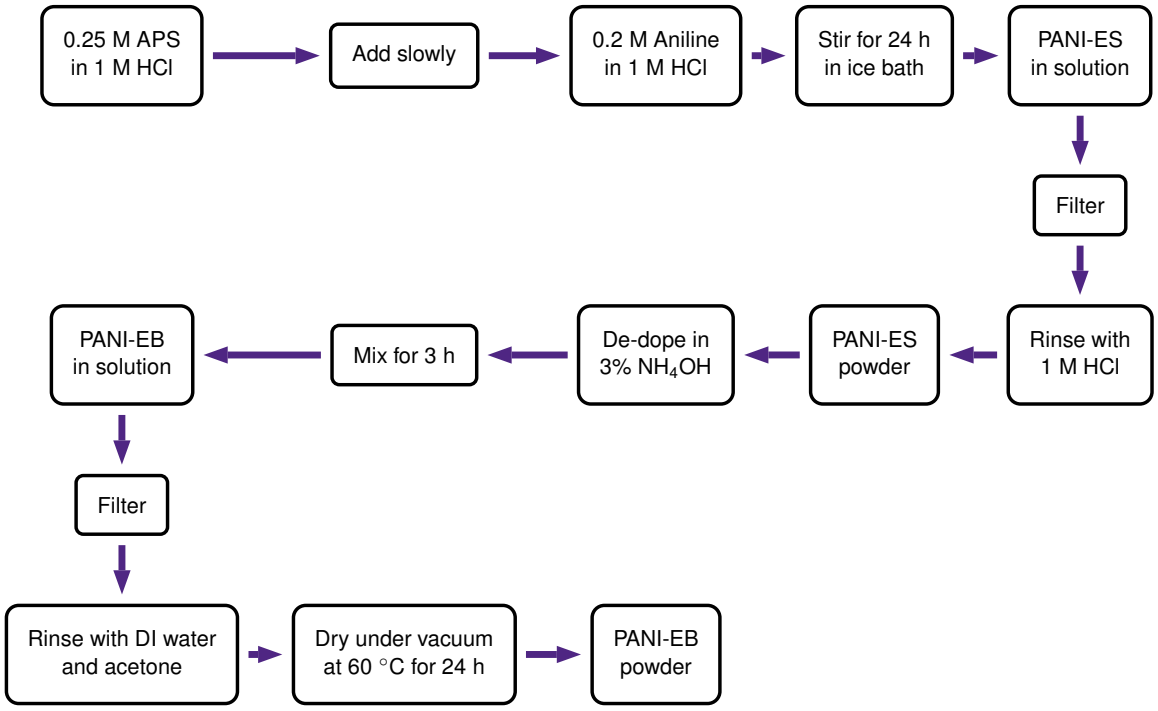

Figure 3.1: This schematic details the chemical oxidative polymerization procedure to synthesize PANI.

ployed due to its ability to achieve scalable batches of PANI powder. The general polymerization process involves the creation of aniline radicals in a low pH solution and addition of an oxidizing agent to propagate the polymer chain and add dopant ions. The polymerization process followed has been based upon IUAPAC suggested process presented by Stejskal and Gilbert (2002) and is illustrated schematically in Figure 3.1. The molar ratio of aniline to APS of 1:1.25 is used based on electron transfer from the persulfate ion and to prevent over-oxidation (Armes and Miller, 1988). A 0.4 M solution of aniline (99%, Sigma Aldrich) is prepared in 1 M hydrochloric acid solution as well as a 0.5 M solution of APS (reagent, Sigma-Aldrich) in 1 M HCl, when combined, these solutions will reach the desired concentrations of 0.2 and 0.25 M respectively. A low-pH solution is required for efficient polymerization PANI in order to form the anilinium cation. Both solutions are placed in ice baths with the aniline solution positioned on a magnetic stirrer and mixed at 350 rpm. Reaction temperature has been shown

to affect the molecular weight of the product, where lower temperatures can achieve higher molecular weights (Mullen et al., 2013). The polymerization is performed near 0 °C to achieve a balance of molecular weight, which can improve some properties of PANI, and processability, high molecular weights can lead to gelation (Mottaghitalab et al., 2006). Once both solutions have reached $0 - 4$ °C, the APS solution is slowly added to the aniline. Initially the solution develops a light pink colour demonstrating the formation of an intermediate stage, then it transitions to a deep blueish purple due to the formation of protonated pernigraniline oxidation state of PANI, and finally a deep green precipitate forms demonstrating the formation of PANI-ES. The polymerization of PANI is an exothermic reaction demonstrating a temperature rise of approximately 12 °C before being cooled back to the original reaction temperature. Following the addition of the APS solution the reaction is left to progress for 24 h under stirring. After the reaction is complete, the green PANI-ES solution is filtered through a buchner filter with VWR 413 filter paper with 5 μm particle retention. Vacuum filtration was employed to quicken the filtering process. The precipitate is then rinsed with 1 M HCl to remove any residual monomer, and other reaction products. The precipitate obtained is PANI in its conductive ES state, however, it is doped with HCl and partially with hydrogen sulfate due to participation of the oxidant in the polymerization. To have the ability to choose a different dopant ion the PANI must be de-doped into the insulating EB oxidation state. To de-dope the PANI the precipitate is mixed with a 3% ammonium hydroxide solution for 2 hrs. The solution is filtered again, yielding a deep blue product, indicating successful transition to the EB state. The precipitate is rinsed with deionized water and acetone to remove reaction intermediates and oligomers (Roichman et al., 1999). Finally, the PANI-EB precipitate is dried under vacuum at 70 °C overnight. The dried PANI-EB is ground with a mortar and pestle and passed through a fine sieve ensure any large particles can be processed further.

The yield of this reaction was found to be relatively low at approximately 65%. This

Material	Cost $[\$/g]$
PANI-EB (in-house)	1.55
PANI-EB (sigma-aldrich)	$13.00 - 53.00$
PANI-ES (sigma-aldrich)	11.30

Table 3.1: Material cost of PANI comparing in-house synthesis and purchasing from commercial chemical suppliers.

loss may be partially attributed to the filtering process, where fine particles may pass through the paper as well as material remnants adhered to the paper. It may also be possible to improve the quality of the reaction; during the first filtering stage the filtrate typically displayed a mild red-pink colour. This colouration can suggest the presence of soluble oligomers or over-oxidized PANI, and is usually caused by excess oxidant in the reaction (Stenhouse, 1864). This should not have a significant impact on the quality of PANI but has impacted the yield. However, the relatively low yield of the reaction still provides drastic cost savings, Table 3.1. Depending on the molecular weight of the PANI purchased from chemical suppliers the cost can vary but savings of over $10 per gram are easily achieved and will only increase with improved reaction yields. These cost estimations are limited to material costs and do not include the cost of equipment or labour. However, the only equipment required is a balance, magnetic stirrer, and glassware which are generally available in a well-equipped research lab. Additionally, the strong dependence on polymerization process parameters and materials can have a large impact on the resultant PANI properties. By maintaining full control over the production of working material the properties of the material can be tuned specific for the development of this new fabrication method and could introduce future research questions (i.e. the effect of molecular weight on conductivity of structures PANI structures fabricated by AM).

3.2 PANI-DBSA paste preparation

Now that PANI has been obtained in its EB oxidation state the polymer can be re-doped with any choice of dopant. To take advantage of the previously discussed counterion-induced thermal doping method, DBSA is used as the dopant. To prepare the PANI-DBSA paste first 5 g of PANI are added to 15 g of DBSA, this 1:3 mass ratio has been adopted to reduce excess DBSA in the final complex (Price et al., 2010). Excess DBSA acts as a plasticizer that may improve extrusion of the paste but will also be water soluble which could limit applications of fabricated devices. Initially the PANI must be dispersed by hand with a small spatula because due to the density difference between the materials a dry, dirt-like mixture is obtained. With sufficient manual mixing the PANI is incorporated throughout the DBSA forming the core-shell structure previously discussed, at this stage a viscous paste is obtain but it is a non-uniform dispersion. To improve the homogeneity of the paste it is mechanically mixed with an overhead stand mixer (Eurostar Control 100) and a dissolver blade. The paste is mixed for approximately 8 min at 850 rpm until a uniform paste is achieved. In the counterion-induced thermal doping method heat is required to initiate the chemical complexation of the constituents; during these initial mixing stages, no heat is added other than frictional heat generated by the stand mixer, thus it is assumed there is minimal doping at this stage in the process. To initiate the doping process the PANI-DBSA paste is mixed further on a hotplate at 100 °C for a prescribed amount of time. During initial testing, it became clear that without any heated mixing the paste had too low of viscosity to support its own weight and allow for fabrication of 3D structures. However, the precise effect of heating on PANI-DBSA paste has not yet been explored.

3.3 PANI-DBSA paste characterization

3.3.1 Methodology

One of the key contributions of this work is the elucidation of the rheological behaviour of PANI-DBSA at different stages of the thermal doping process. In many direct ink writing applications, there is a mechanism available to control the flow characteristics of the material, by adjusting the composition, for example, increasing the viscosity by increasing the percentage of an additive. In this case, it is desirable to maintain the same composition based on stoichiometric ratios but the flow characteristics may be controlled by controlling the degree of doping in the paste. In the development of this AM technique for PANI it is essential to understand how the doping reaction affects the flow properties of the material and how they can be used in extrusion based applications. Previous reports have identified a paste to solid transition, as well as optimal temperatures to complete the thermal doping reaction, but by analyzing the rheological behaviour after various heating times then optimal conditions may be determined to prepare PANI-DBSA paste for AM extrusion methods. It has been reported by Titelman et al. (1997) that below 120 °C, the thermal doping reaction will not be fully completed, thus to investigate formulations that have not fully reacted a lower temperature, 100 °C, has been used. Future studies may investigate the effect of temperature on the doping reaction and eventually transition to analyzing heat energy and rates per gram of the material to normalize the process for a range of batch sizes.

The aim of this study was two-fold; first, to identify a rheological model describing the flow characteristics of the material in response to various shear rates. Secondly, material subjected to various amounts of heated mixing were tested to develop an empirical model to describe the effect of thermal doping time on the flow characteristics of the material. Additionally, the paste viscosity, and shear rate dependence can impact the required extrusion pressure as well as the likelihood of post extrusion deforma-

tion. An initial rheological study was conducted using a Rheometrics stress rheometer, configured in the parallel plate geometry. To assess the material's shear strain rate dependence, a dynamic strain sweep was conducted from $0.1 - 100$ rad/s at 1% strain. This test was repeated for mixtures heated for 2, 3, 4, and 5 min, with 3 tests conducted at each thermal doping time.

3.3.2 Results and discussion

Following the rheometry study, the paste flow was found to follow the Ostwald shear-thinning power law model:

$$\eta = \eta_0 \dot{\gamma}^{n-1}, \tag{3.1}$$

$$\log \eta = (n-1) \log \gamma + \log \eta_0, \tag{3.2}$$

where η_0 is the consistency constant that describes the viscosity of the fluid at a shear rate of 1 s^{-1}, and n, the power law index (Coussot, 2005). When this model is analyzed on the log scale, the power law index describes the slope of the line and the consistency constant determines the y-intercept (Equation 3.2). It was also shown that an increase in heating time of the PANI-DBSA results in an increase in viscosity (Figure 3.2). This increase in viscosity was expected as demonstrated by the aforementioned research introducing the paste-to-solid transition. Curve fitting was performed in MATLAB using nonlinear least squares and robust bisquare regression to determine the consistency factor and power-law index for each heating time. The robust method applies a degree of outlier rejection by searching for a model that fits the majority of data and assigning a lower weight to data farther from this curve (Rousseeuw and Hubert, 2011). The 3 data sets obtained for each thermal doping time were combined to obtain representative power law coefficients for each time. Flow behaviour at each heating time was captured well by the power law model with r^2 values greater than 0.98 for each thermal

doping time above 0 min. The unheated sample had an r^2 value of 0.94, and while this is a relatively good fit, the heating process may have promoted improved dispersion as well as chemical complexation. Thus, without any pre-extrusion thermal doping applied, the paste was less homogenous and more likely to exhibit wider variations in flow properties. Once the power-law coefficients corresponding to each heating time were determined, the relationship between the coefficients and pre-extrusion thermal doping time, in minutes, were found empirically. For η_0 as a function of time, a 1-term exponential function was used with the addition of a *y*-offset. Similarly, the relationship between *n* and pre-extrusion heating time was fitted to a 2-term exponential function. Using these forms, the coefficients were determined for each variable and the relationship is described by Equations 3.3 and 3.4 for η_0 and *n* respectively,

$$\eta_0 = 0.0685e^{2.0587t} + 36.233 \tag{3.3}$$

$$n = 0.5531e^{-0.01434t} - 4.23 \times 10^{-7}e^{2.719t}. \tag{3.4}$$

Together these equations describe the flow behaviour of the paste in terms of heating time and shear rate. This study shows an agreement with previous research suggesting a distinct paste-to-solid transition. For this specific case, 20 g of material heated at 100 °C, there appears to be an increase in viscosity initiated at approximately 3 min and a sharp increase after 4 min. This transition was also observed during paste extrusion, where material heated for 3 min or less had a tendency to flow under its own weight. During rheological characterization, it was determined that the material heated for 5 min was nearly solid due to the thermal doping reaction being near completion and therefore, the material was not extrudable. The analyzed heating times provide an overall view of the curing reaction at 100 °C that displays how the viscosity is changing at stages of this reaction. Further investigation should focus on the 3–5 min range to

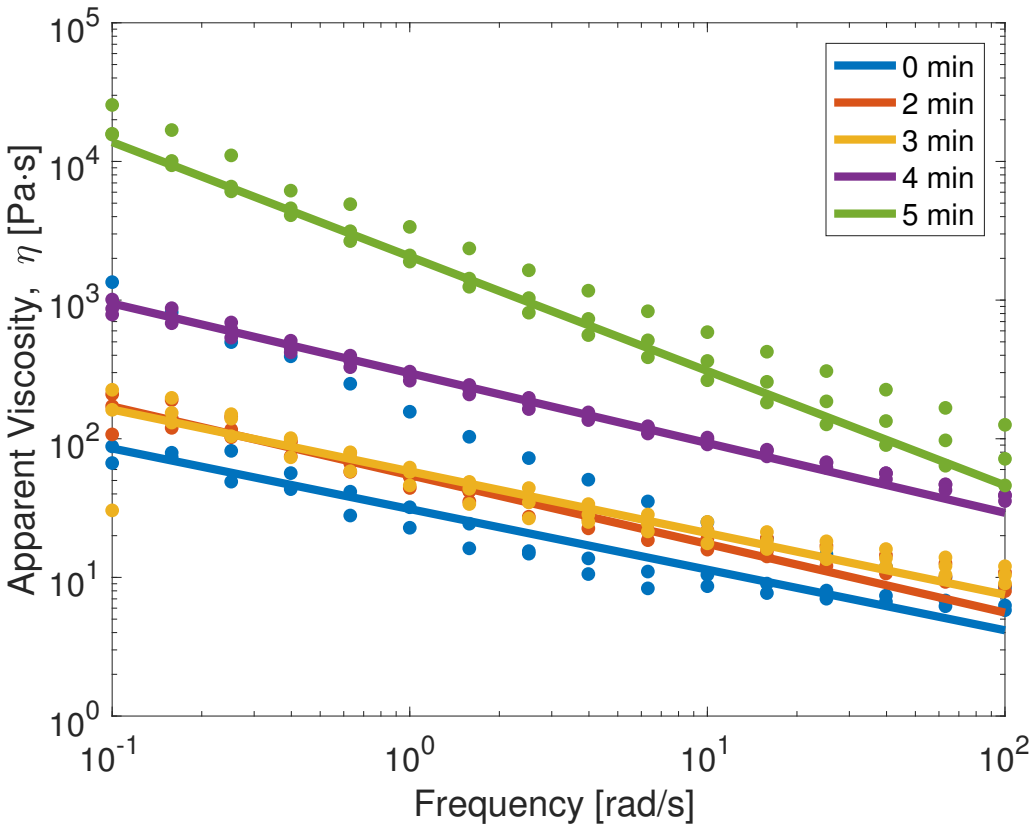

Figure 3.2: Shear-thinning behaviour is observed for PANI-DBSA paste heated at 100 °C for different durations demonstrated the expected increase in viscosity with thermal doping time.

assess the accuracy of the empirical model in this critical range.

3.4 Chapter summary

This chapter outlined the chemical oxidative polymerization of PANI-ES, and de-doping into PANI-EB in preparation for CITD with DBSA. The preparation procedure of PANI-DBSA paste was presented and the rheological behaviour of the paste was characterized. A rheological study was conducted which determined PANI-DBSA flow can be modelled by the Ostwald shear-thinning power law. Additionally, this study investigated the impact of thermal doping time on the flow properties of PANI-DBSA paste to de-

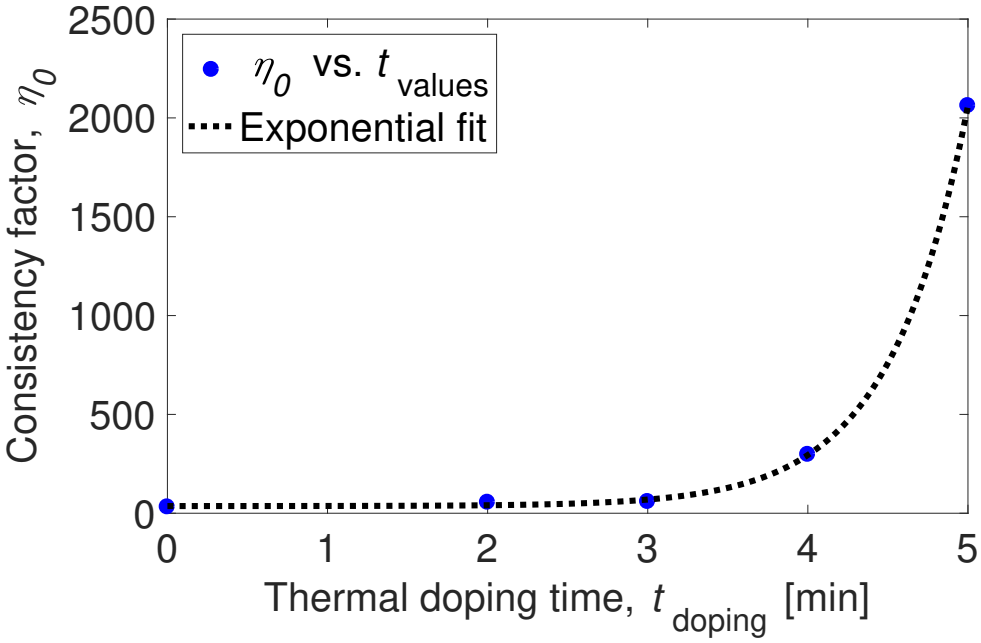

(a) Reference viscosity

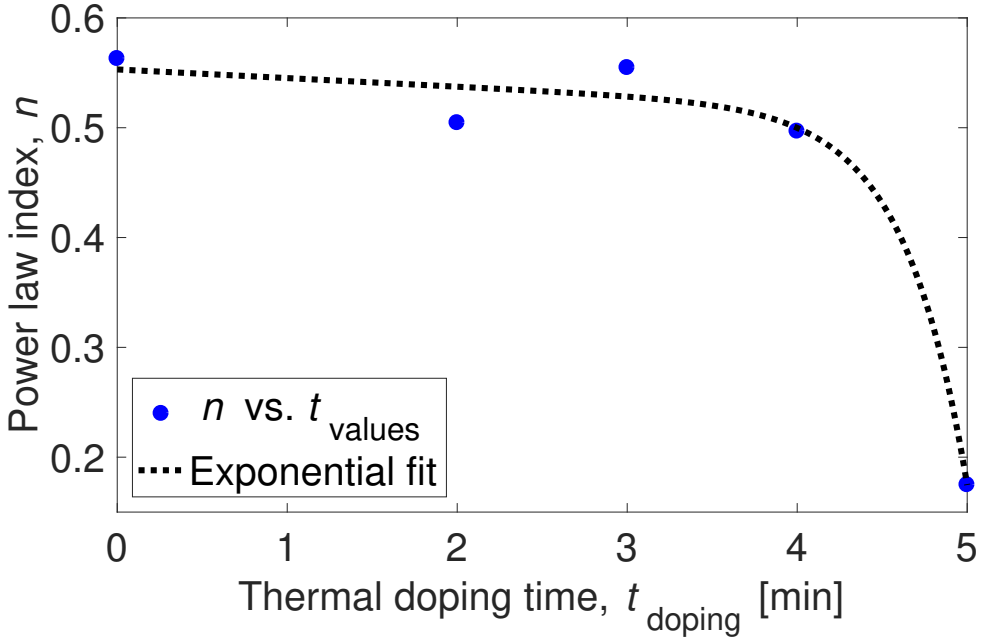

(b) Power law index

Figure 3.3: The experimentally determined power law coefficients as a function of heating time for PANI-DBSA paste are captured by the proposed exponential relationships.

velop empirical models describing the power law coefficients as a function of thermal doping time. This understanding of the flow behaviour of PANI-DBSA paste can now be applied to an extrusion model to provide designers with a tool to select application specific process parameters.

List of references

Armes, S. P. and Miller, J. F. (1988), 'Optimum reaction conditions for the polymerization of aniline in aqueous solution by ammonium persulphate', *Synthetic Metals* **22**(4), 385–393.

Coussot, P. (2005), *Rheometry of Pastes, Suspensions, and Granular Materials*, John Wiley & Sons, Inc., Hoboken, NJ.

Mottaghitalab, V., Spinks, G. M. and Wallace, G. G. (2006), 'The development and characterisation of polyaniline—single walled carbon nanotube composite fibres using 2-acrylamido-2 methyl-1-propane sulfonic acid (AMPSA) through one step wet spinning process', *Polymer* **47**(14), 4996–5002.

Mullen, K., Reynolds, J. R. and Masuda, T., eds (2013), *Conjugated Polymers*, RSC Polymer Chemistry Series, The Royal Society of Chemistry, Cambridge, GBR.

Price, A. D., Kao, V. C., Zhang, J. X. and Naguib, H. E. (2010), 'Fabrication and percolation behaviour of novel porous conductive polyblends of polyaniline and poly(methyl methacrylate)', *Synthetic Metals* **160**(17–18), 1832–1837.

Roichman, Y., Titelman, G., Silverstein, M., Siegmann, A. and Narkis, M. (1999), 'Polyaniline synthesis: influence of powder morphology on conductivity of solution cast blends with polystyrene', *Synthetic Metals* **98**(3), 201 – 209.

Rousseeuw, P. J. and Hubert, M. (2011), 'Robust statistics for outlier detection', *Wiley Interdisciplinary Reviews: Data Mining and Knowledge Discovery* **1**(1), 73–79.

Stejskal, J. and Gilbert, R. G. (2002), 'Polyaniline. Preparation of a conducting polymer(IUPAC Technical Report)', *Pure and Applied Chemistry* **74**(5), 857–867.

Stenhouse, J. (1864), 'Action of chloride of iodine on certain organic substances', *Journal of the Chemical Society* **17**, 327–332.

Titelman, G. I., Zilberman, M., Siegmann, A., Haba, Y. and Narkis, M. (1997), 'Thermal dynamic processing of polyaniline with dodecylbenzene sulfonic acid', *Journal of Applied Polymer Science* **66**(12), 2199–2208.

Wallace, G. G., Spinks, G. M., Kane-Maguire, L. A. and Teasdale, P. R. (2009), *Conductive Electroactive Polymers: Intelligent Polymer Systems*, 3rd edn, CRC Press, Boca Raton, FL.

Chapter 4

Direct ink writing apparatus development and process modelling

In conjunction with the development and characterization of PANI paste formulations a multi-material DIW apparatus for the fabrication of high-resolution 3D PANI-based structures was developed. Initially a syringe pump paste extrusion system was employed to provide a proof of concept demonstration and encounter any major issues with the process. Issues with paste flow controllability led to the adoption of a CNC pneumatic valve that was integrated with the conventional FFF delta printer to obtain a multi-material extrusion apparatus. Previous knowledge of PANI-DBSA paste flow properties was combined with an extrusion model to predict the width of extruded tracks. The model validation was conducted to provide the designer with a basis to modify vital fabrication parameters such as print speed, pressure, and nozzle diameter to enable the design of high-resolution 3D conductive PANI structures. Further development of this model is required to account for post extrusion flow resulting in track widening, and a more focused investigation on the change in flow properties during the critical paste to solid transition exhibiting during the PANI-DBSA thermal doping process. Finally, sample structures were presented to highlight the ability of the system to created multi-layered

high-resolution PANI-DBSA structures.

4.1 Apparatus development

4.1.1 Fused filament fabrication delta robot

The framework for this fabrication system is provided by a commercially available FFF 3D printer in a delta configuration, as opposed to cartesian. In this configuration, there are 3 independent stepper motors driving carriages along vertical rails, where each carriage is connected to the end effector by rigid arms and a ball joint or spherical bearings, Figure 4.1. The combination of vertical displacements of these carriages controls the position of the end effector in the *x*-*y* plane and a simultaneous movement of each carriage results in a displacement in the *z*-axis. The key advantages to the delta configuration is the low inertia of the moving parts allows for superior accuracy at higher print speeds, quiet operation, and an automatic bed levelling feature. The delta kinematics are programmed into the printer's firmware (Bell, 2015). The firmware employed is a branch of the open-source firmware "Marlin" designed for FFF 3D Printers using delta configurations [†].

The 3D printer is controlled by the Azteeg X3, an arduino based 3D printer controller. This board is designed specifically for additive manufacturing applications and provides all the essential ports and connections for position drive motors, extruder drive motors, heating elements for the hot end and heated bed, and cooling fans. The printer is shipped with the necessary wiring and components to extrude a single material through a single hot end, but the board is designed for expansion to integrate an additional extruder motor and hot end. The as-shipped printer is specified to have a layer resolution of 100 μm. The smallest realizable feature is not specified but feature resolution has

[†] reprap.org/wiki/Marlin

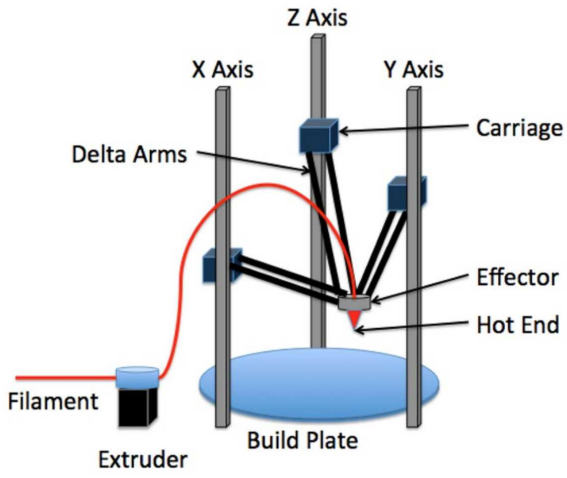

Figure 4.1: Schematic of the standard configuration for delta 3D printers (© Bell, 2015, included with permission).

been found to be highly dependent upon the selected process and geometry of the feature. The combination of open-source software and expandable/modular hardware allows for rapid modifications and retooling of the system for different applications. For example, improving the resolution of the positioning stepper motors may realize finer feature and layer resolutions.

4.1.2 General AM process

During the development of this process many changes were made, however the general procedure remained the same and can be split into 4 main steps: paste preparation, model and G-code preparation, paste extrusion, and post-extrusion thermal doping. As discussed in Chapter 3 the paste extrusion step involves dispersing the PANI in DBSA and mixing under applied heating to initiate thermal doping, effectively controlling the flow characteristics of the paste. Next, a 3D model is produced, using 3D CAD software, and imported to a commercial slicing software, where essential process parameters are specified, from which, the tool paths and extrusion information are generated. Once the tool paths are produced and the material is prepared, the structure can be

fabricated using the CNC delta robot for position and a paste extrusion tool for material deposition. It is important to note that at this point the material has only been partially doped and remains in paste form. To finalize the complexation of the PANI and DBSA a post-extrusion thermal doping process is required by applying heat to the sample, this additional heating results in a paste-to-solid transition and an increase in the conductivity of the material (Zilberman et al., 1997). These steps were under concurrent development during the project and modifications were made to each step throughout, however, the framework of the procedure remained consistent.

4.1.3 Initial paste extrusion system

As discussed above, the 3D printer was only equipped with a single conventional filament extruder and hot end. Initial proof of concept for direct ink writing of PANI-based pastes was achieved through the integration of an aftermarket paste extruder. The paste extruder design was similar to a syringe pump where a material cartridge is loaded into the device and extrusion is controlled by a geared stepper motor driving a lead screw. The key advantage to this system is that minimal modifications were required to the existing printer for successful integration of the paste extruder. Since the paste extruder is driven by a stepper motor the device can be directly connected to the extruder output of the printer. A configuration parameter in the 3D printer firmware is the steps per mm of the stepper motors, this value can be specified for both the position and extruder drive motors. This value controls the number of steps required for the stepper motor to move either 1 mm or extrude 1 mm of filament, and by adjusting this value based on the motor steps per revolution, driver microstepping, and gear ratio, the new extruder can be calibrated. Fine calibration calculations for this design were not completed because of the exploratory nature of the testing. Instead a rough calibration was achieved by specifying a steps per mm value suggested by the paste extruder manufacturer, followed by adjusting a parameter in the slicing software for fil-

ament diameter for finer adjustment of the extrusion rate. This method was effective because the volume of extruded material is calculated by both the length and diameter of the filament; by decreasing the filament diameter the extrusion rate will increase to achieve the same volume flow rate and vice versa. With the fabrication of the mounting clamp for a nozzle and the installation of tubing to connect the nozzle to the cartridge the paste extruder integration was completed, Figure 4.2.

This apparatus enabled the relatively quick proof of concept towards the fabrication of 3D conductive PANI structures, characterization of these structures, and identification of any potential limitations in the system or material design. Following refinement of the fabrication parameters the ability to create multi-layered structures was achieved and the conductivity of these structures were analyzed, Figure 4.3. Additionally, this allowed the initial examination of the effect of post fabrication thermal doping to finalize the complexation of the PANI-DBSA paste and improve its conductivity. However, while this system provided valuable experience in development of the fabrication process it presented some limitations and challenges. The slow speed of the leadscrew driven system and the expansion of the tubing that ran from the syringe pump base to the end effector affected the controllability of the paste flow. As a result, there was an inherent lag in the paste extrusion resulting in a disparity between the actual and the modelled extrusion position. This lag also created challenges for multi-material printing where the paste material would ooze from the nozzle while not in use. The tubing also resulted in wasted material that could not be extruded. Finally, this system was prone to clogging, while this is partially attributed to insufficient extrusion pressures, the paste preparation process was also under development and agglomerations of particles may have contributed to clogging as well.

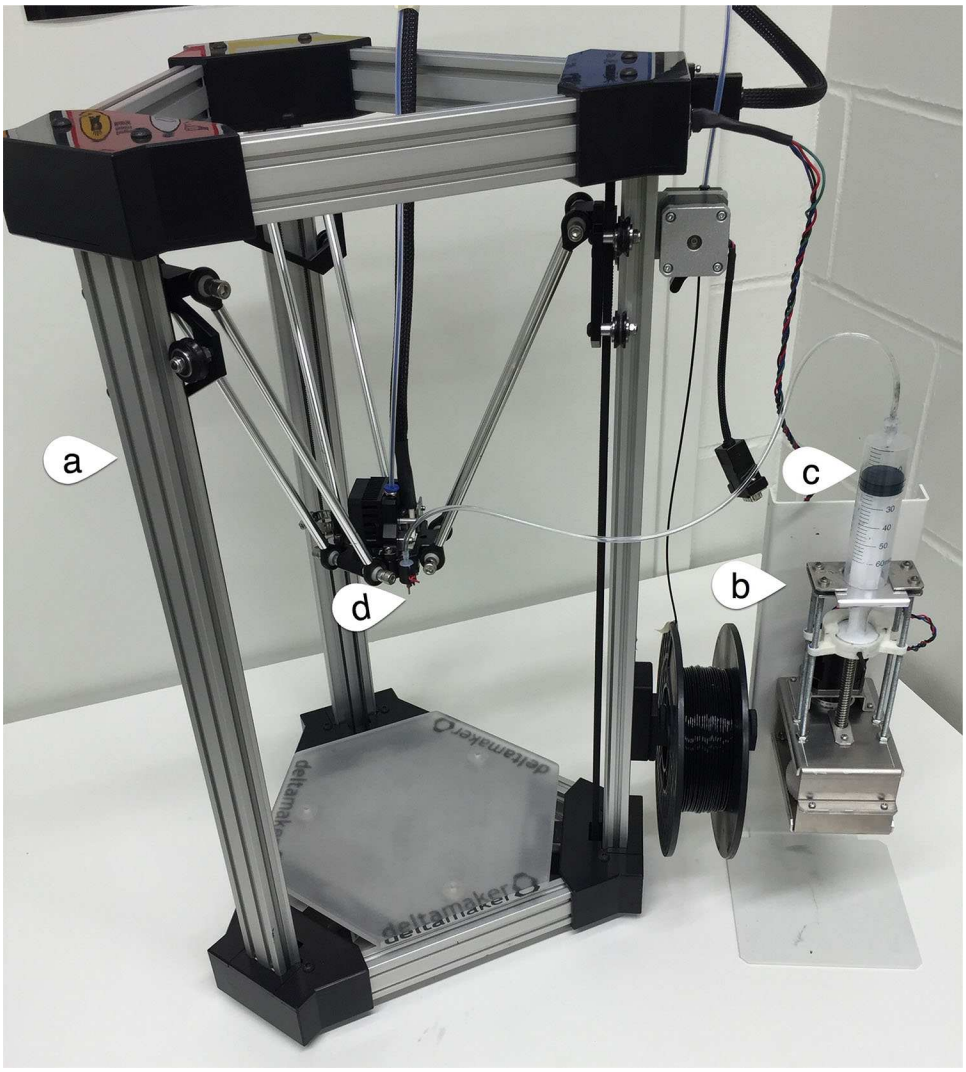

Figure 4.2: Fabrication apparatus consisting of (a) modified fused filament fabrication delta robot, (b) integrated paste extrusion system, (c) polymer paste cartridge, and (d)paste extrusion nozzle (© Holness and Price, 2016, included with permission).

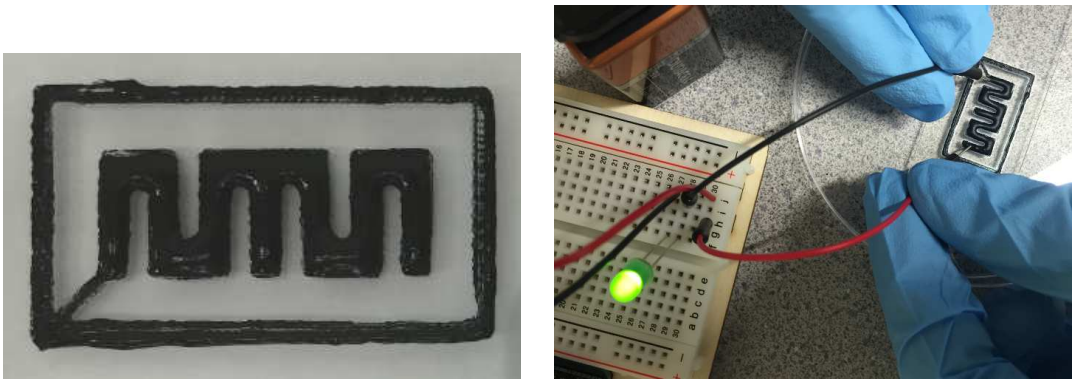

(a) (b)

Figure 4.3: (a) A fabricated PANI-DBSA structure prior to post-extrusion thermal doping, and (b) demonstration of electrical conductivity on the thermally doped sample (© Holness and Price, 2016, included with permission).

4.1.4 Final paste extrusion system

To correct the material waste and flow control issues, the syringe pump system was replaced with a computer controlled pneumatic valve (Nordson EFD). The maximum output pressure of the pneumatic valve is 100 psi and with the addition of a high pressure tool this can be scaled to 400 psi. This system provided increased accuracy in paste deposition through discrete bursts of high pressure air providing a highly controllable flow. Additionally, the material barrel was able to be mounted directly on the end effector, adjacent to the conventional hot end, eliminating the effect of expanding tubing. Typical FFF systems use stepper motors to drive the filament through the hot end, this required the output signal to be modified for communication with the pneumatic valve. To integrate the pneumatic valve with the delta robot an auxiliary microcontroller was added to read the standard stepper motor output and relay the signal to the digital I/O port on the pneumatic valve to initiate and terminate an extrusion cycle Figure 4.4. To initiate an extrusion the microcontroller reads the step and direction outputs from the 3D printer controller. If a high signal is detected for both step and direction pins a voltage is applied across the requisite pins of the pneumatic valve I/O port. This allows the use of conventional slicing software to generate tool paths coupled with

extrusion data while capitalizing on the advantages of the pneumatic paste extrusion system. Sampling the direction pin was required because it is possible for retractions to be commanded during the G-code preparation stage. A retraction is a AM technique where the extruder direction is reversed to pull the filament out of the hot end a small degree, this prevents unwanted material from oozing out of the nozzle when executing travel moves. However, the pneumatic valve doesn't recognize this feature and without sampling the direction pin the paste extruder would only receive a step command and extrude unnecessarily. If a retraction signal is detected, by switching of the direction pin, a voltage is applied across the alarm pins of the pneumatic valve terminating the extrusion. The complete pneumatic valve integration microcontroller program is available in Appendix A.2. The extrusion pressure is selected directly through the internal controller on the pneumatic valve and is calibrated as a function of nozzle diameter, print speed, and the paste's apparent viscosity (Suntornnond et al., 2016).

The as-purchased 3D printer was not intended for paste extrusion or dual extrusion, as such, the original bulky hot end design and limited mounting space did not allow for integration of an additional extruder. To mount both a conventional hot end and paste extrusion tool, a significantly smaller hot end was purchased and mounting brackets were designed for the new hot end, paste extrusion tool, and bed levelling components were fabricated. These brackets were produced by FFF for speed of production and ease of design iteration, however, a final design could be produced using higher strength materials. One challenge in the design of the paste extruder mounting bracket was the requirement to adjust the z-position of the tool. This requirement was driven by the variation in disposable nozzle lengths. The current design allows the user to loosely clamp the paste extrusion tool, manually adjust its z-position, and fully clamp it into position. These modifications have enabled improved achievable line resolutions of approximately 250 μm, compared to the syringe pump system, and the ability to accurately control paste deposition enabling multi-material extrusion. The multi-material

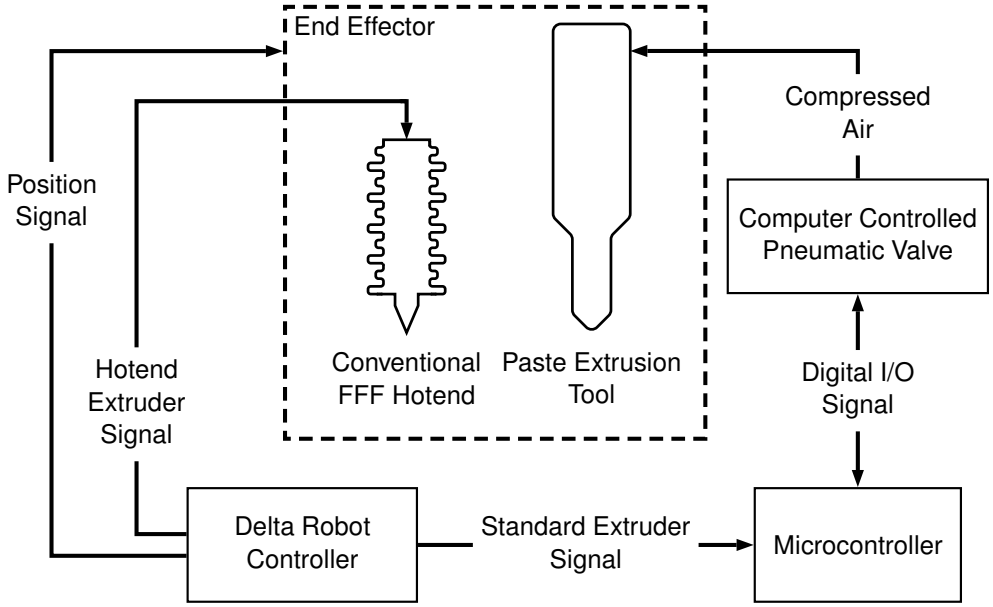

Figure 4.4: Schematic of multi-material extrusion direct ink writing system (© Holness and Price, 2017, included with permission).

extrusion system combines a standard FFF hot end with the ability to print conventional AM filament materials up to 245 °C, and while the focus of the paste extrusion tool is to enable direct ink writing of PANI based compositions, there are no limits to the range of fluids for which its use may be envisioned. Finally, the open-source nature of the components used in this system provides low-level control of the entire process enabling a high degree of modularity and adaptation for future design improvements, including in situ thermal doping of PANI based formulations, non-planar tool paths, and installation of additional paste extruders.

4.1.5 G-code preparation and modification

One of the challenges in multi-material AM is the different material properties require different printing parameters for successful extrusion. This issue is addressed in the slicing software, Simplify3D. This software allows designers to import multiple STL files to the workspace and define unique process parameters for each model. This enables

process optimization on a material specific level while minimizing any trade-off due to the multi-material process. However, the slicing software and printer controller do not allow for the definition of unique steps per mm settings for each extruder, to overcome this challenge the G-code file is generated with two tools defined and is processed by a python script (Appendix A.1). This script prompts the user to select the desired G-code file and define the steps per mm for each tool. The script then searches the file for instances of tool changes and inserts a line of code redefining the global steps per mm setting following each tool change.

4.2 PANI-DBSA extruded track width study

4.2.1 Model development

After development of the PANI-DBSA paste, fabrication apparatus, and G-code preparation, further refinement of the process was required. A previous model was developed by Suntornnond et al. (2016) to predict the track width of extruded bioinks under various process parameters. Using the shear stress developed during capillary flow (through the nozzle), the volume flow rate can be determined by an assumption that a constant geometry track is deposited for a given nozzle speed. Combining this assumption with the power law model for shear thinning fluids discussed in Chapter 3, the relationship between process parameters and fluid viscosity is given by:

$$d\left(v,\Delta P\right)=D^{2}\sqrt{\frac{1}{32\eta L}\cdot\left(\frac{4n}{3n+1}\right)\cdot\frac{\Delta P}{v}}, \tag{4.1}$$

where, D, L, η, n, ΔP, and v represent nozzle diameter, nozzle length, apparent viscosity, power law index, gauge pressure, and nozzle travel speed respectively. The track width is shown to be directly proportional to the square root of the gauge pressure and

inversely proportional to the square root of the travel speed:

$$d \propto \sqrt{\Delta P}, \tag{4.2}$$

$$d \propto \sqrt{\frac{1}{v}}. \tag{4.3}$$

From the constant geometry assumption, the shear rate of the material through the nozzle can be estimated by:

$$\dot{\gamma} = \frac{4n}{3n+1} \cdot \frac{2v}{D}, \tag{4.4}$$

where n is determined from the recently developed relationship between thermal doping time and flow properties, v is the print speed, and D is the nozzle diameter (Suntornnond et al., 2016). Following the calculation of the shear rate, the apparent viscosity of the paste can be calculated using the empirical models defining the shear thinning behaviour as described in Chapter 3. At this point all the relevant parameters are known and the expected track width can be calculated.

4.2.2 Methods

To verify that the previously developed model can be extended to PANI-based pastes and that the heating time effect can be accurately incorporated in the model, a study of extruded tracks was conducted with material heated for 3.5 and 4 min where tracks were deposited over a range print speeds and pressures. Extrusion speeds and pressures were selected based on estimations from the track width model and due to changes in material properties were dependent upon thermal doping time. Material heated for 3.5 min was extruded at print speeds of 5, 10, and 15 mm/s and gauge pressures of 200, 240, 280, 320, and 360 psi. Material heated for 4 min was extruded at a print speed of 4 mm/s and gauge pressures of 280, 320, 360, and 400 psi. The prescribed extrusion path was as a continuous track with 5-parallel lines as shown in

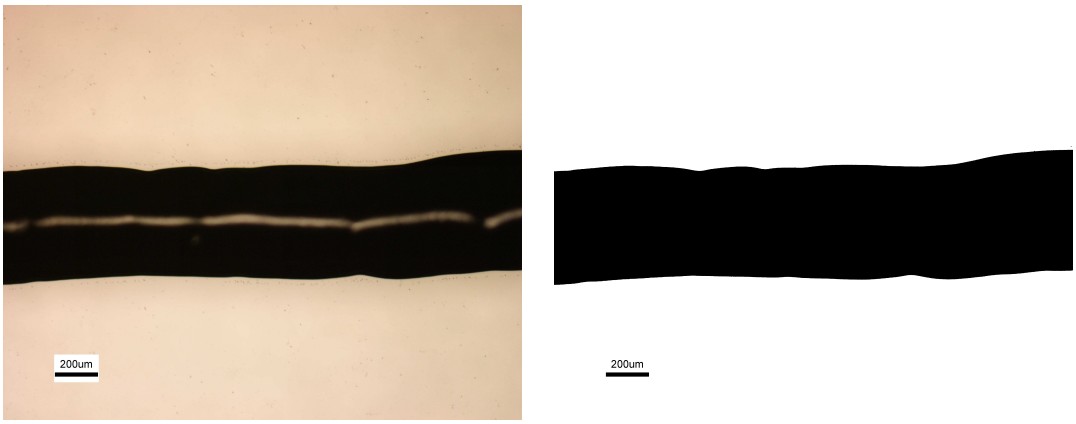

(a) (b)

Figure 4.5: (a) An unmodified image of an extruded track and (b) the same image following preprocessing in preparation for track width measurement.

Figure 4.7a. One width measurement was taken on each of the 3 central lines of a single part extruded each combination of extrusion parameters. Extruded tracks were analyzed via optical microscopy (Nikon Eclipse L150), and obtained images were processed in ImageJ to determine the average track widths. To reduce the time required to process the images a more automated workflow was employed that took advantage of an open-source macro for ImageJ. This macro automatically identifies the edges of the track and calculates the average track width as well as the roughness of the edges. However, it was found that the edges could be more easily identified if the image was converted to black and white. Following initial image processing the track widths could be accurately identified and measured, Figure 4.5.

4.2.3 Results and discussion

The first validation of the model focused on extrusion of PANI-DBSA for a single thermal doping time, as shown in Figure 4.6a. Material with the same flow properties was extruded at various print speeds and gauge pressures to test the model's ability to handle those two print parameters. The model predicts the track width for speeds of 10

and 15 mm/s for all pressures demonstrating r values of 0.81 and 0.82 respectively. While this model does not provide an exact prediction of the expected track width it does provide the designer with a reasonable estimate from which process parameters can be adjusted experimentally. In calculation of r values for 15 mm/s the tracks extruded at 15.5 $\sqrt{psi}$ were excluded because they were determined to be artificially high due to non-characteristic effects, possibly due to a temporary nozzle blockage resulting in pressure buildup. As can be seen in Figure 4.6a, at 5 mm/s print speed there was better agreement between the model and experimental results at low extrusion pressures. In addition, at this print speed the model increasingly under-predicts track width as the pressure increases. This disagreement is assumed to be caused by over-extrusion, where the extruded track no longer maintains the assumed circular cross section. If the vertical distance between the nozzle and substrate is small, then during over-extrusion the nozzle becomes buried in extruded material and excess material is forced outwards. This results in an extruded track with an elongated cross section that is wider than it is thick. A future improvement to the model may be to modify the geometry of the cross-section to account for the distance between the nozzle and the substrate. Until future model refinements are applied, the limitations of the model may be checked by comparing the predicted track width to the diameter of the nozzle. Initial results suggest that tracks predicted to be significantly wider than the nozzle diameter cannot be accurately reproduced experimentally.

The next parameter studied was the ability to account for different pre-extrusion thermal doping times. Due to the significant change in viscosity between the samples heated for different lengths of pre-extrusion thermal doping it was not possible to test at the same pressures and speeds without encountering over- or under-extrusion in one set of samples. Figure 4.6b shows the experimental and predicted track widths for tracks extruded after 3.5 and 4 min of the thermal doping at 100 °C. There was less agreement between the model and experimental data for tracks extruded after 4 min

heating, especially at low extrusion pressures, demonstrating an r value of only 0.57. The disagreement at low extrusion pressures may be due to pressure losses in the system resulting in an extrusion pressure lower than the gauge pressure. The overall poor correlation could suggest a change in the paste flow behaviour due to the paste to solid transition during the thermal doping reaction. A large change in viscosity was seen between 3 and 4 min of thermal doping and it is possible that this large change in viscosity cannot be accounted for by the model in its current form.

Examples of extruded tracks in Figure 4.7 highlight how the change in process parameters has significant impact on the extrusion track width. For example, tracks extruded at 360 psi but at 5 and 10 mm/s, Figure 4.7c and d respectively show a large change in track width that ultimately could not be accounted for by the model. Finally, inconsistent extrusion occurred at 10 mm/s at 70 psi possibly caused by agglomerations in the paste suggesting improvements to the paste preparation process are required. A potential route to improve the accuracy of the track width model is to consider a more representative cross-sectional geometry of the extruded tracks. For example, Turner and Gold (2015) have proposed a rectangular cross-section for the extrusion of thermoplastics which considers the width and thickness of the extruded road. This model also identifies the acceleration of the end effector as a contributor to over and under extrusion leading to variations in extruded track widths, Figure 4.8. This effect has been limited by measuring the track widths along long, steady extrusions. However, future refinements of the model will focus on identifying the cross-section geometry and controlling the extrusion pressure as a function of end effector acceleration.

4.3 Sample 3D PANI-based structures

This fabrication process, from modelling the material flow to iterations of the extrusion system, has been driven by the goal of producing high-resolution conductive PANI-

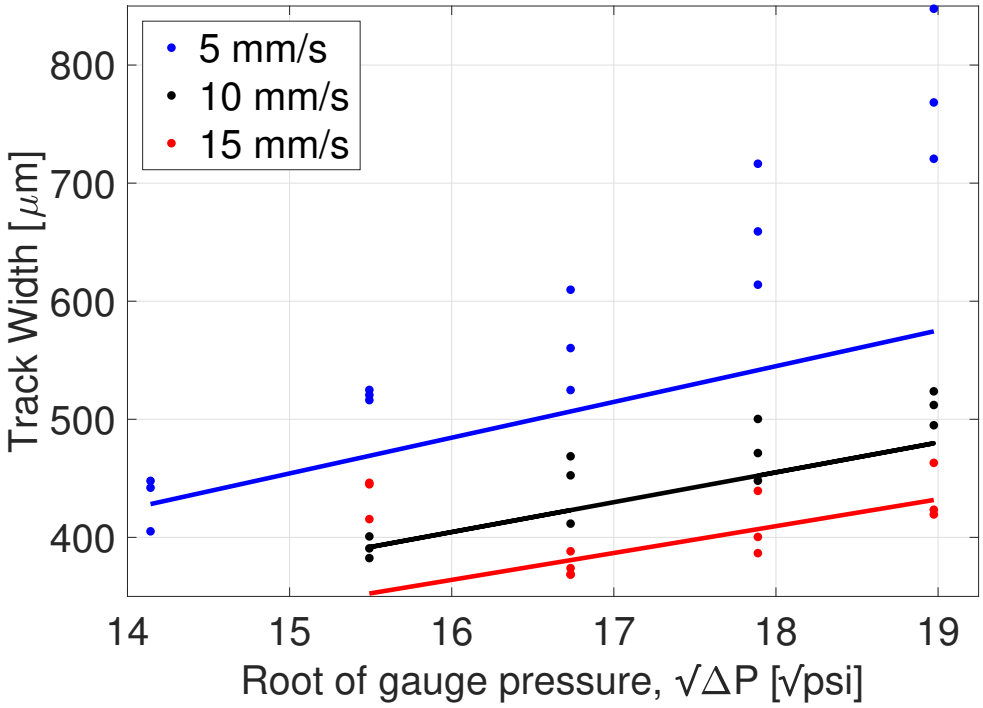

(a) 3.5 min thermal doping

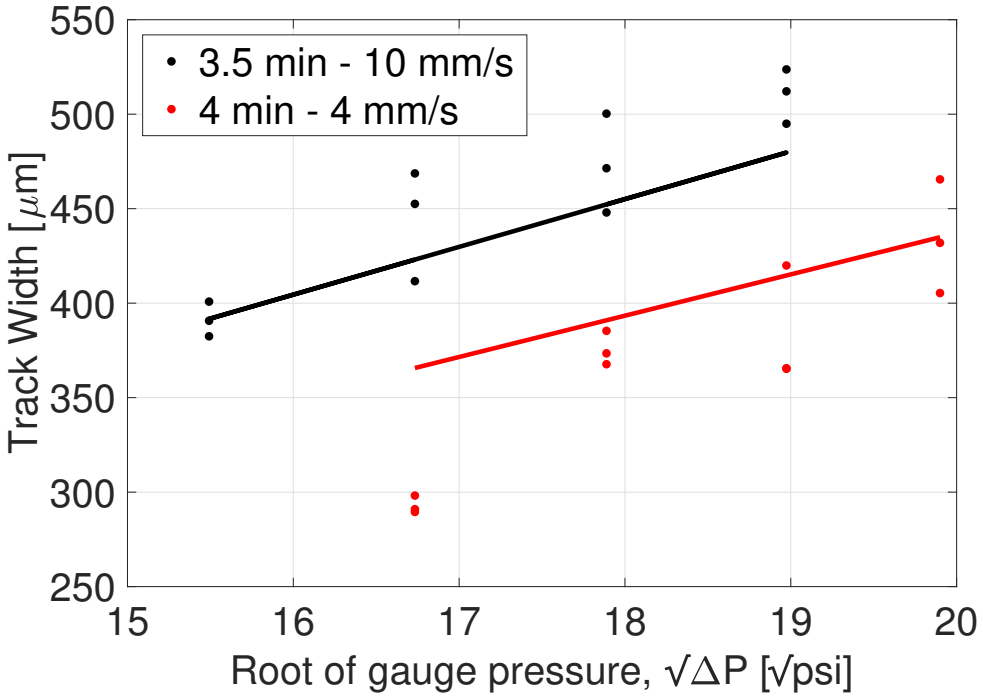

(b) 3.5 and 4 min thermal doping

Figure 4.6: Experimentally observed track widths (points) extruded at a range print speeds for paste heated for 3.5 min and 4 min depart from the prediction curve (solid lines) under non-ideal conditions.

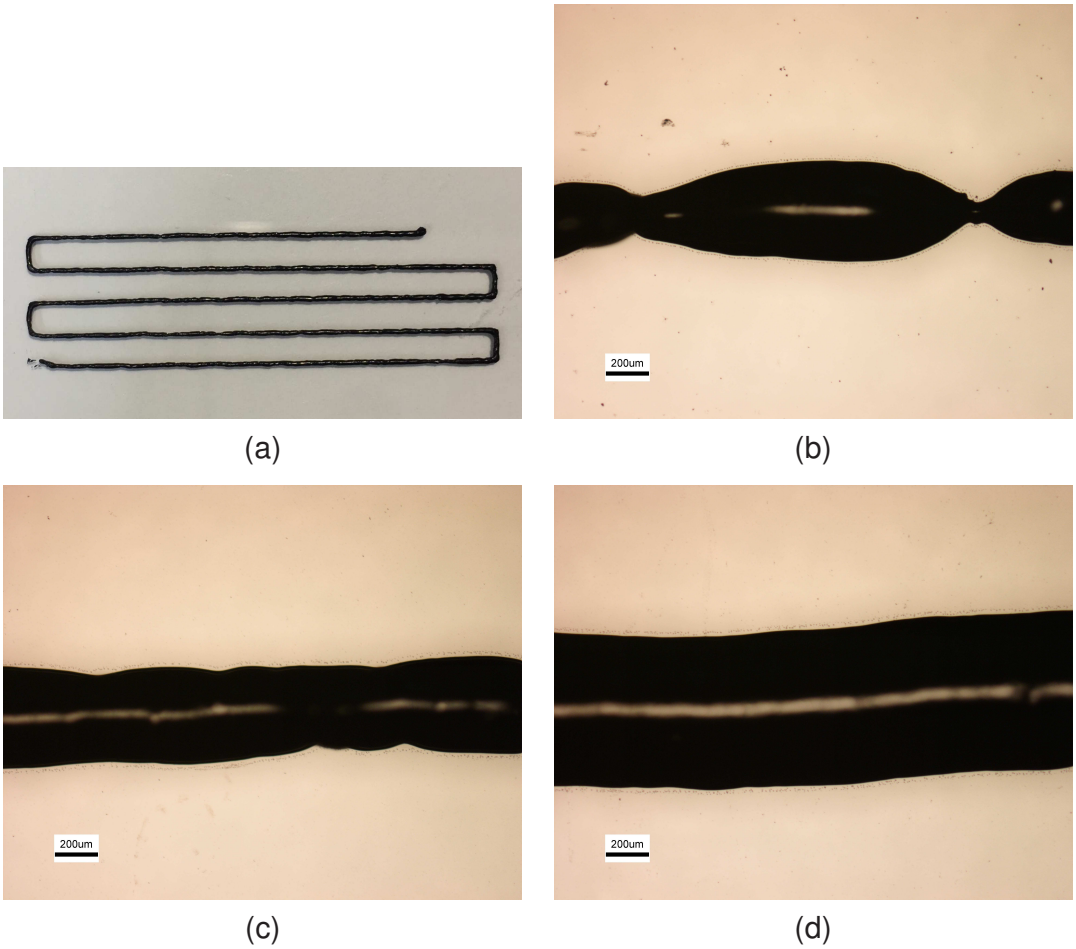

Figure 4.7: A typical extruded track sample (a), and microscope images of inconsistent extrusion (b), consistent extrusion (c), and over extrusion (d).

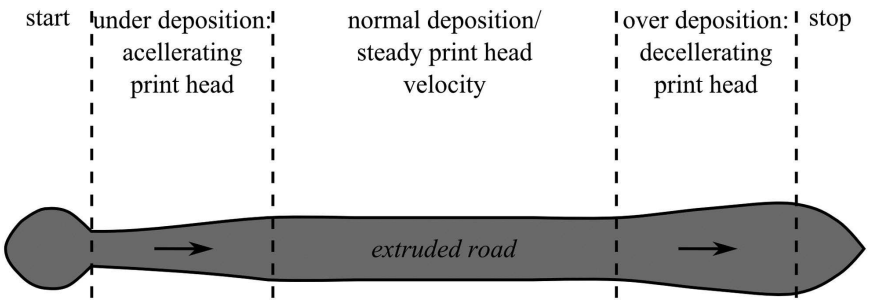

Figure 4.8: Illustration demonstrating the impact of end effector acceleration on track width at the beginning and end of an extrusion (© Turner and Gold, 2015, included with permission).

based structures. Figure 4.9 shows examples of the features realizable by the extrusion system in its current state. In these examples the ability to create multi-layered structures is highlighted as well as fine features such as sharp corners.

4.4 Chapter summary

This chapter outlined the development of a multi-extrusion DIW apparatus for the fabrication of high-resolution 3D PANI-based structures. Initially, a syringe pump paste extrusion system was explored and allowed for a proof of concept towards the successful production of 3D PANI structures. Issues with paste flow controllability led to the adoption of a CNC pneumatic valve that was integrated with the conventional FFF delta printer to obtain a multi-material extrusion apparatus. Previous knowledge of PANI-DBSA paste flow properties was combined with an extrusion model to predict the width of extruded tracks. The model validation was conducted to provide the designer with a basis to modify vital fabrication parameters such as print speed, pressure, and nozzle diameter to enable the design of high-resolution 3D conductive PANI structures. Further development of this model is required to account for post extrusion flow resulting in track widening, and a more focused investigation on the change in flow properties during the critical paste to solid transition exhibiting during the PANI-DBSA thermal doping process. Finally, sample structures were presented to highlight the ability of the system to created multi-layered high-resolution PANI-DBSA structures.

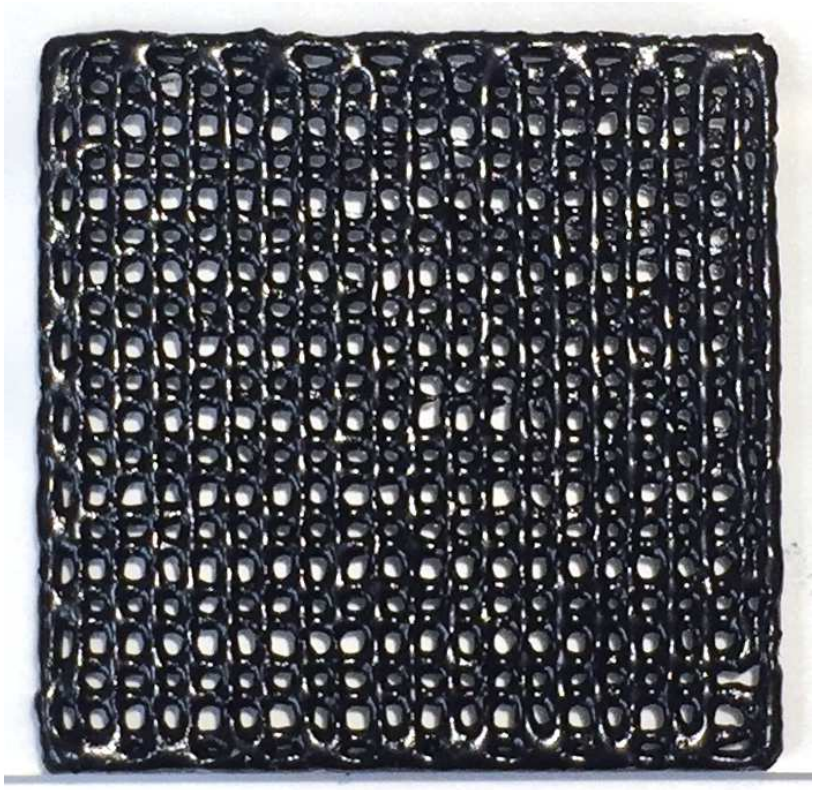

(a) 2-layer grid

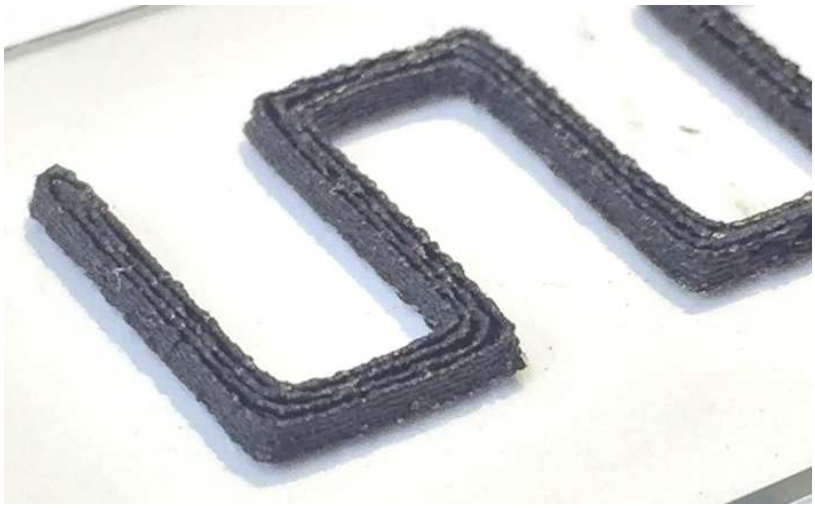

(b) 5-layer S-pattern

Figure 4.9: The direct ink writing process for polyaniline has been employed to 3D print multilayered (a) 20 mm $\times$ 20 mm piezosensor mats and (b) printing test patterns to assess the viability of the process for the fabrication of fine features such as sharp corners. The prescribed layer height is 200 μm, and the width of the S-pattern is approximately 2 mm.

List of references

Bell, C. (2015), *3D Printing with Delta Printers*, Apress, New York, NY.

Holness, F. B. and Price, A. D. (2016), Robotic extrusion processes for direct ink writing of 3D conductive polyaniline structures, *in* Y. Bar-Cohen and F. Vidal, eds, 'SPIE Smart Structures and Materials + Nondestructive Evaluation and Health Monitoring', SPIE, pp. 97981G–97981G–8.

Holness, F. B. and Price, A. D. (2017), Design and fabrication of conductive polyaniline transducers via computer controlled direct ink writing, *in* Y. Bar-Cohen, ed., 'Proceedings of SPIE - The International Society for Optical Engineering', Western University, London, Canada, SPIE, p. 101632O.

Suntornnond, R., Tan, E., An, J. and Chua, C. (2016), 'A Mathematical Model on the Resolution of Extrusion Bioprinting for the Development of New Bioinks', *Materials* **9**(9), 756–11.

Turner, B. N. and Gold, S. A. (2015), 'A review of melt extrusion additive manufacturing processes: II. Materials, dimensional accuracy, and surface roughness', *Rapid Prototyping Journal* **21**(3), 250–261.

Zilberman, M., Titelman, G. I., Siegmann, A., Haba, Y., Narkis, M. and Alperstein, D. (1997), 'Conductive blends of thermally dodecylbenzene sulfonic acid-doped polyaniline with thermoplastic polymers', *Journal of Applied Polymer Science* **66**(2), 243–253.

Chapter 5

Application of PANI in embedded piezoresistive strain sensor by multi-material AM techniques

This chapter outlines the first ever study of a PANI-based piezeoresistive strain sensor fabricated by the in-situ embedding of the conductive PANI material in a flexible TPE support material. The sensor is characterized by measuring the change in resistance while longitudinal strain is applied. The sensor performance was assessed through analysis of the gauge factor and sensor stability was investigated through cycling the applied strain. Additionally, the effect of post-extrusion thermal doping time on the piezeoresistive response of the sensor is analyzed.

5.1 Introduction

Since the relatively recent discovery of the intrinsic piezoresistive properties of PANI, there has been further application of PANI to transducers and actuators capitalizing on this effect (Lillemose et al., 2008; Pereira et al., 2012; Della Pina et al., 2014; Falletta

et al., 2014). However, these devices are typically fabricated using conventional 2D film deposition techniques and while there have been significant advances in these techniques, performance of these devices may benefit from the ability to fabricate complex 3D conductive PANI structures. The realization of these structures is achieved through the implementation of a modified FFF delta robot equipped with an integrated computer controlled pneumatic valve for extrusion of high viscosity polymeric formulations. Herein, an initial study of the piezoresistive response of a 3D embedded PANI-based strain sensor is reported. This sensor was fabricated via a multi-material extrusion process combining computer controlled direct ink writing of PANI-based pastes with conventional additive manufacturing techniques to deposit passive and active structures concurrently. The process parameters utilized during sensor fabrication were informed by the extruded track width model developed in Chapter 4. The design of this sensor was focused on initial assessment of the piezoresistive effect of the PANI-DBSA formulation The impact of post fabrication thermal treatment on the performance of the devices has been investigated in terms of the gauge factor and stability.

5.2 Methods

5.2.1 Sensor fabrication procedure

The sensor was modelled with overall dimensions of 12 $\times$ 60 $\times$ 1.8 mm where a rectangular prism of PANI-DBSA paste (4 $\times$ 60 $\times$ 0.6 mm) is deposited in the center of the sensor that is fully encompassed by the support material, (Figure 5.1a). In this test, the support material was composed of a commercial TPE with a yield strength of 9 MPa at 55% elongation. This material provided a compliant substrate and support to induce strain at relatively low loads. Conventional 3D printing slicing software was used to generate the toolpaths for the respective materials by constructing a separate 3D model for each material. This software also provided the ability to control all other relevant

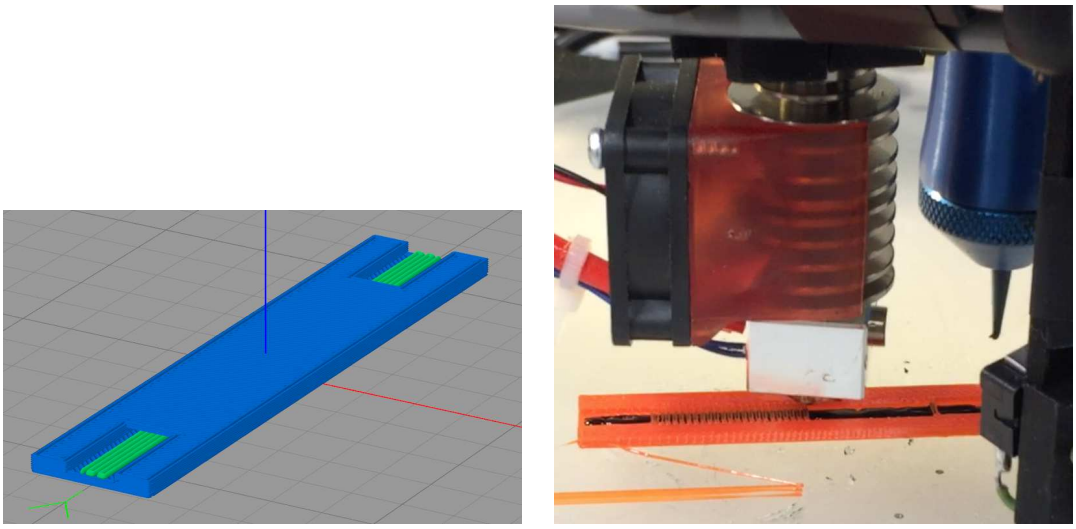

(a) (b)

Figure 5.1: (a) Modelled sensor after processing in slicing software and (b) sensor during fabrication demonstrating embedding of PANI-DBSA paste in TPE support (© Holness and Price, 2017, included with permission).

parameters, including print speed, layer heights, nozzle diameter, and infill percentage to consider the limitations imposed by material properties. The support material was extruded with a layer resolution of 200 μm, nozzle diameter of 400 μm, and print speed of 20 mm/s. Whereas the PANI-DBSA was deposited with a layer resolution of 600 μm, nozzle diameter of 430 μm, and print speed of 10 mm/s. Following modelling, G-code preparation and calibration, the device is fabricated through concurrent extrusion of the PANI-DBSA paste and TPE support material (Figure 5.1b). A higher resolution paste deposition layer height is achievable in single material processes, but fabrication parameters require further calibration to realize these layer resolutions during multi-material processes.

5.2.2 Post-extrusion thermal doping

Following fabrication, samples were heated on a hotplate at 120 °C for 2.5 and 5 min respectively. This heating finalizes the thermal doping process and allows for character-

ization of the electromechanical impact of different post-extrusion thermal doping times. Additionally, a silver epoxy was applied to provide an electrical contact with the testing apparatus; future designs will attempt to use extruded PANI-DBSA as the electrode.

5.2.3 Sensor performance characterization

To assess the piezoresistive performance of these sensors, longitudinal strain was applied by a custom rubber stretching apparatus composed of a stepper motor driven leadscrew and carriage mounted on linear rails, Figure 5.2. The system contained electrical contacts integrated in the sample clamps and the contacts were connected to a Keithley 2611 SourceMeter for resistance measurement. The stepper motor control was provided by Anaheim Automation DPN10601 programmable drivers. Resistance measurements were recorded in 4-wire sensing mode with pairs of current and voltage electrodes. A constant DC voltage of 5 V was applied for all samples. Cyclical loading of the sample to 1% strain was applied at 0.1% intervals with resistance measurements recorded at each step after a delay of 1 s to allow for the sensor to stabilize. This process was repeated for 40 cycles to assess the stability of the sensor. To quantify the performance of the sensors, the gauge factor has been calculated by:

$$GF = \frac{\Delta R/R_0}{\Delta l/l_0} = \frac{\Delta \rho/\rho_0}{\varepsilon} + 1 + 2\nu, \tag{5.1}$$

where the change in resistance due to geometric effects can be separated from the intrinsic piezoresistivity of the material (Falletta et al., 2014). R_0 is assigned to the first resistance recorded at 0% strain on the first cycle and is also used as the reference to determine ΔR. A limitation of the stretching apparatus software was that resistance measurements could only be recorded during extension of the sample and not during relaxation. For the initial characterization of these sensors, this limitation is acceptable; however, Falletta et al. (2014) demonstrated a variation in gauge factor during exten-

sion compared to relaxation. Therefore, future analysis will consider the change in resistance of the device during both stretching and relaxation to assess any significant hysteresis.

5.3 Results and discussion

Samples heated for 5 min demonstrated a higher DC resistance than samples heated for 2.5 min. This higher resistance suggests that the longer post-extrusion heating time resulted in the samples being over cured, causing mechanical degradation, and brittle structure. Figure 5.3 demonstrates the sampling procedure on a typical sample during the stretching cycle with the data points representing resistance measurements recorded during the first 2 stretching cycles. During the first stretch, there is an increase in the relative change in resistance until it reaches a peak at the maximum 1% strain at which point the sample is relaxed to its initial length without taking any electrical characterization and the stretching cycle is repeated. Figure 5.4 shows the normalized change in resistance over 40 loading cycles for devices subjected to each post-extrusion thermal doping time to assess the stability of the devices. Both heating times showed a trend towards steady operation where the normalized resistance at 0% strain increased with cycle number. Future studies should be conducted with higher cycle numbers to provide more accurate characterization of longterm stability and performance of the sensor. Additionally, the change in resistance for each cycle decreased to a more steady value. The device heated for 2.5 min demonstrated larger changes in normalized resistance than the 5 min device. While the 5 min device exhibited a smaller change in resistance, it reached a state of consistent performance faster than the 2.5 min device. The overall trend in both samples may be explained by the formation of many new cracks in the initial stages of cycling until a sufficient state of stress relaxation was achieved where minimal new cracks formed and crack propagation was

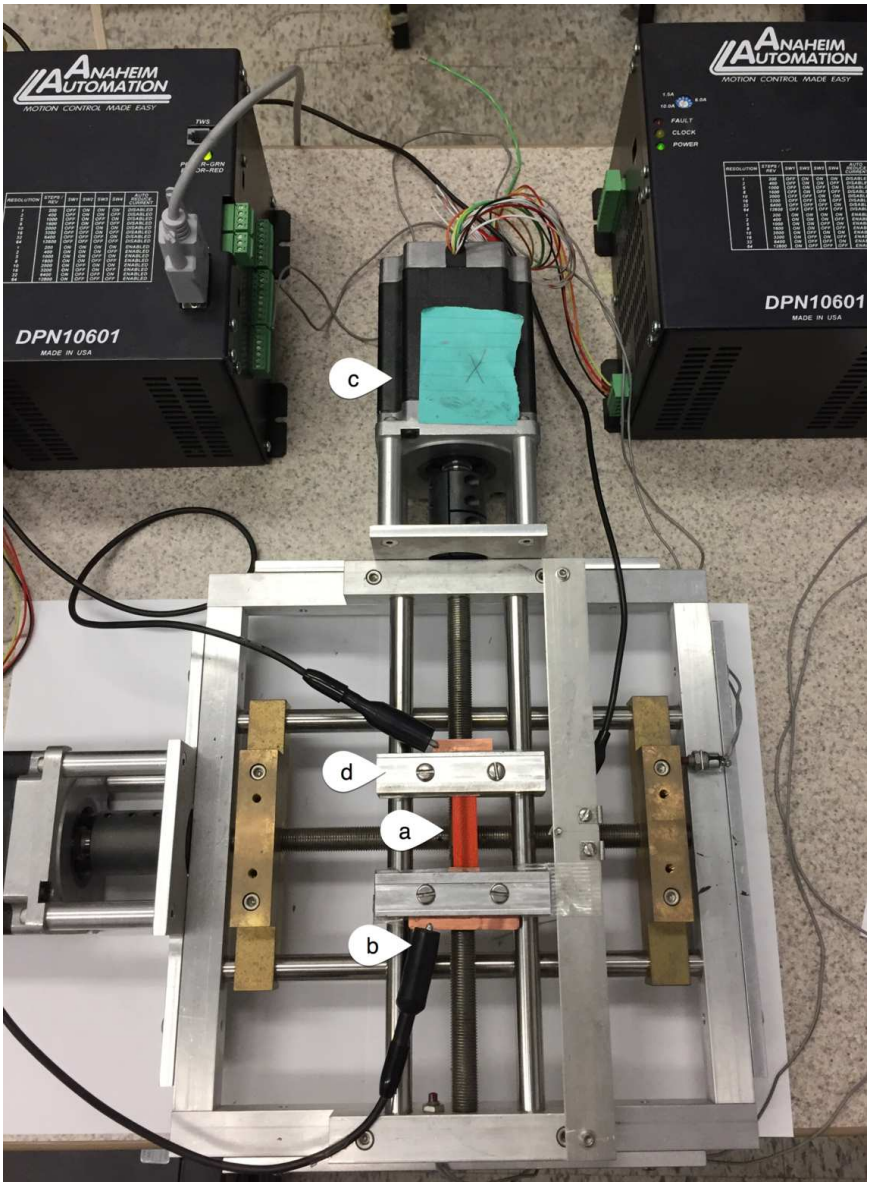

Figure 5.2: Strain sensor characterization was conducted on custom stretching apparatus consisting of: (a) a mounted PANI-DBSA sensor, (b) integrated electrical contacts for *in situ* measurement of piezoresistive response, (c) driven stepper motor, and (d) linear carriage assembly.

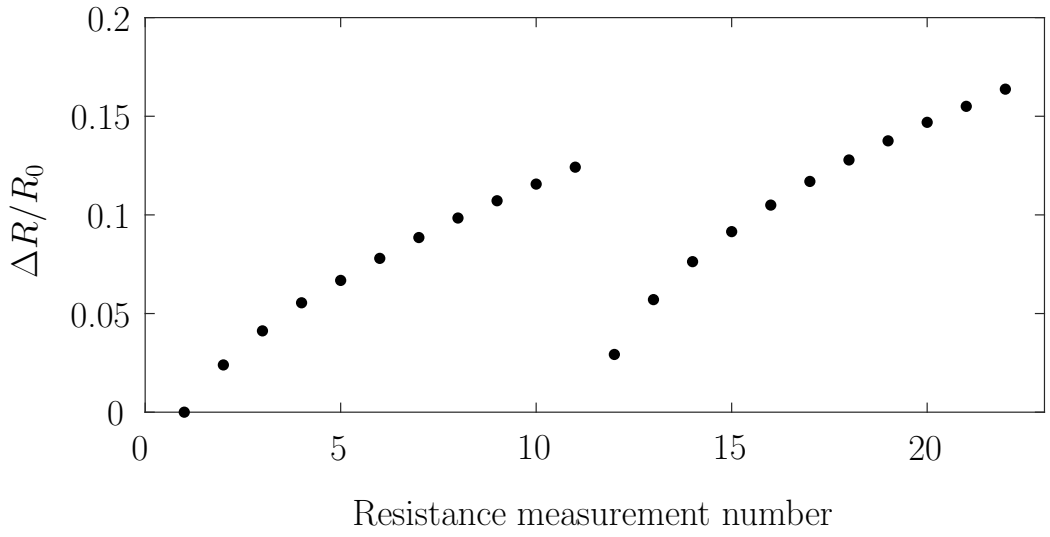

Figure 5.3: The resistance response during the first 2 stretching of a PANI-DBSA strain sensor heated at 120 °C for 5 min with the data points representing measurements recorded during the stretching cycles and peaks representing the end of a cycle.

minimal. The faster trend towards stability for the 5 min sensor may be due to its more brittle structure being more susceptible to cracking thus reaching steady performance faster. It is anticipated that with extended cycling the 2.5 min sensor would also reach steady performance. Previous studies have shown that temperature effects can cause a change in electrical and mechanical properties of PANI (Pud, 2003). These changes can include an additional mechanical degradation that results in the annealing of the amorphous phase providing improved order and an increase in conductivity (Davenas and Rannou, 1999). Future sensor design will focus on the post-fabrication thermal doping parameters to identify their effect on PANI-DBSA microstructure and the optimal heating time and temperature for sensor performance.

The gauge factors have been estimated by fitting a linear regression to the normalized resistance versus strain plots for the last 5 cycles from each final thermal doping heating time across the range 1% strain loading cycle (Figure 5.5). While the linearity of the device performance was poor, the response was repeatable throughout cycling, especially in later cycles. The last 5 cycles were used in calculating the gauge fac-

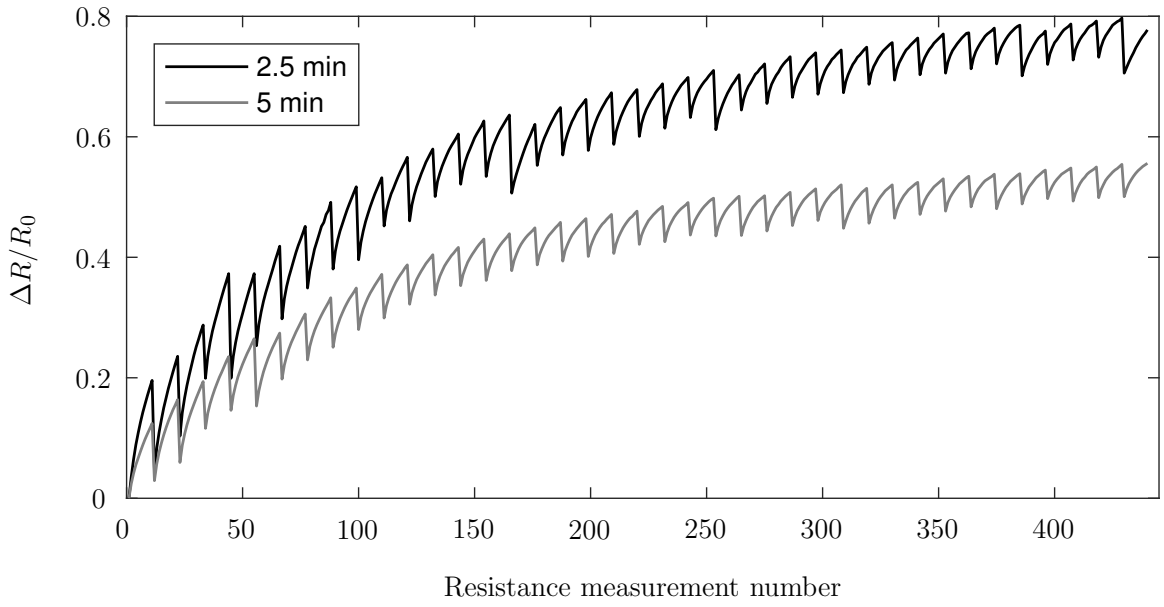

Figure 5.4: Stability of sensors over 40 loading cycles for samples heated at 120 °C for 2.5 and 5 min. No lag was observed between mechanical loading and the electrical response at the imposed loading rate (© Holness and Price, 2017, included with permission).

tor because in the early cycles the gauge factor decreased with the formation of new cracks until the device stabilized. In both devices, the early cycles still exhibited nonlinear behaviour but there was a significant change in the gauge factor between cycles. For the 2.5 min sensor, the standard deviation of the normalized change in resistance at 1% strain for the first 5 cycles is 0.080 compared to 0.0093 for the last 5 cycles. Similarly, for the 5 min sensor, the standard deviation of the first 5 cycles was 0.056 and only 0.0045 for the last 5. These variations can be attributed to the early stages of cycling being effected by crack formation under loading, especially at the extreme of the loading cycle, whereas later cycles see fewer new cracks formed and less crack propagation. Figure 5.5 also shows that the 5 min sensor reached more stable performance faster than the 2.5 min sensor based on the proximity of the successive gauge factor curves. Gauge factors of 6.42 (r^2 = 0.715) and 5.09 (r^2 = 0.883) were calculated for 2.5 and 5 min devices respectively. As shown by the r^2 values for the calculated gauge factors, the linearity of the sensor must be improved, and the linear fit was ap-

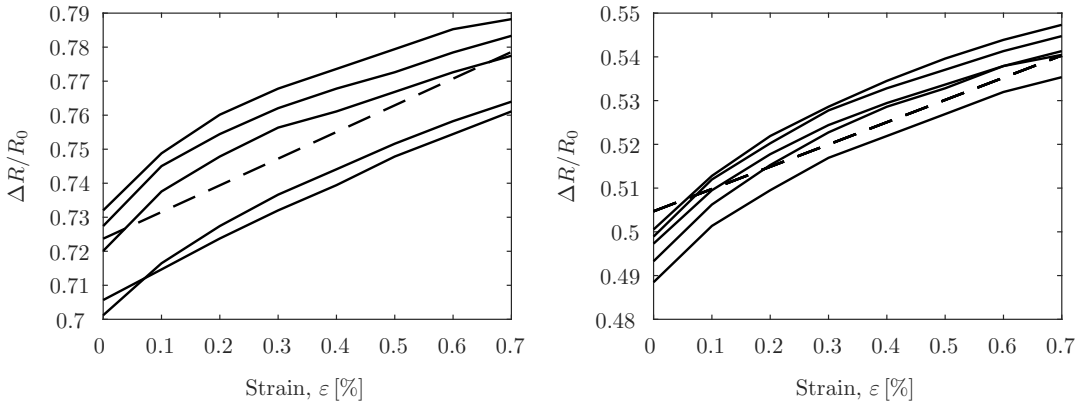

(a) 2.5 min (b) 5 min

Figure 5.5: Device gauge factors computed for the final 5 cycles for final thermal doping at 120 °C for (a) 2.5 min and (b) 5 min (© Holness and Price, 2017, included with permission).

plied only to estimate the gauge factor to assess the potential of these devices for further development. Although slightly lower, these gauge factors are in a similar range of those previously reported by Falletta et al. (2014), and still compare favourably to gauge factors of commercial piezoresistive strain sensors.

To assess the performance of the devices at higher strains and potentially identify a critical failure strain of the device, both final thermal doping time devices were subjected to 5% strain with steps occurring at every 0.5% for 3 cycles. During these tests a critical failure mode was identified as the delamination of the PANI-DBSA complex from the TPE support material (Figure 5.6). This effect may be attributed to interfacial stresses in the material arising from the disparity in mechanical properties of the two materials, including poisson ratio and Young's Modulus. To address this effect a better agreement between the mechanical properties of the active and support materials may be required to achieve higher strains and extend sensor life.

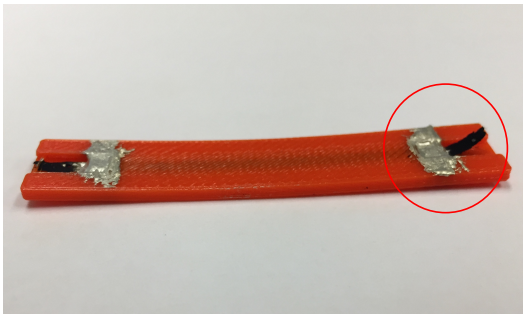

Figure 5.6: Delamination of PANI-DBSA complex from TPE support was observed following 5% strain (© Holness and Price, 2017, included with permission).

5.4 Chapter summary

This chapter has outlined the first ever study of an PANI-based piezeoresistive strain sensor fabrication by the in-situ embedding of the conductive PANI material in a flexible thermoplastic elastomer. The sensor was fabricated using a novel multi-material paste extrusion system enabling the concurrent deposition of passive and active structures. It was shown that these sensors demonstrated an increase in resistance both during a loading cycle and between successive cycles with a trend towards a stable operating point. Additionally, the parameters selected for the final thermal doping process have been shown to have a significant impact on the device performance both in terms of stability and gauge factor. This effect can be attributed to the change in mechanical and electrical properties of the material during the thermal doping process. Finally, the interfacial stresses of the PANI-DBSA and support material must to be studied further to avoid delamination and improve sensor stability. It is clear that the electromechanical performance of these devices will highly depend on the thermal treatment applied after fabrication. Future work will focus on characterizing the effect of post-fabrication thermal doping on PANI-DBSA microstructure and crack propagation during cycling to optimize sensor design for application-specific performance.

List of references

Davenas, J. and Rannou, P. (1999), 'Optical reflectance and RBS studies of thermally aged CSA-protonated polyaniline films', *Synthetic Metals* **102**(1-3), 1283–1284.

Della Pina, C., Zappa, E., Busca, G., Sironi, A. and Falletta, E. (2014), 'Electromechanical properties of polyanilines prepared by two different approaches and their applicability in force measurements', *Sensors and Actuators B: Chemical* **201**, 395–401.

Falletta, E., Costa, P., Della Pina, C. and Lanceros-Méndez, S. (2014), 'Development of high sensitive polyaniline based piezoresistive films by conventional and green chemistry approaches', *Sensors and Actuators A: Physical* **220**, 13–21.

Holness, F. B. and Price, A. D. (2017), Design and fabrication of conductive polyaniline transducers via computer controlled direct ink writing, *in* Y. Bar-Cohen, ed., 'Proceedings of SPIE - The International Society for Optical Engineering', Western University, London, Canada, SPIE, p. 101632O.

Lillemose, M., Spieser, M., Christiansen, N. O., Christensen, A. and Boisen, A. (2008), 'Intrinsically conductive polymer thin film piezoresistors', *Microelectronic Engineering* **85**(5-6), 969–971.

Pereira, J. N., Vieira, P., Ferreira, A., Paleo, A. J., Rocha, J. G. and Lanceros-Méndez, S. (2012), 'Piezoresistive effect in spin-coated polyaniline thin films', *Journal of Polymer Research* **19**(2), 9815–8.

Pud, A. (2003), 'Some aspects of preparation methods and properties of polyaniline blends and composites with organic polymers', *Progress in Polymer Science (Oxford)* **28**(12), 1701–1753.

Chapter 6

Concluding remarks

6.1 Summary of conclusions

This thesis explored the issues surrounding the development of a novel AM method specifically tailored for the fabrication of complex 3D conductive structures of PANI for the fabrication of actuators and transducers. The experience gained/knowledge ascertained through these activities has prompted the following conclusions:

1. The development of a PANI-based paste specifically designed for AM processes was explored. This process entailed the synthesis of PANI from its monomer to maintain control over the material properties of the paste constituents. An empirical rheological model was developed to describe the effect of the counterion-induced thermal doping process on the flow properties of the paste. This model demonstrated that PANI-DBSA paste follows the Ostwald shear-thinning power law and describes the changes in both the consistency factor and power law index as a function of thermal doping time.

2. A novel fabrication apparatus for the extrusion of PANI-based pastes was developed. Through the integration of conventional AM techniques this multi-material CNC extrusion system enables the deposition of high-resolution conductive PANI-

based structures. Functional devices can now be fabricated through concurrent deposition of filament-based passive structures and active PANI structures.

3. A model for the extrusion of PANI-DBSA paste was adapted from an existing model for bio-ink extrusion. This model was extended to incorporate the effect of counterion-induced thermal doping on the flow properties of the paste. This model can be used to predict the width of extruded tracks as a function of fundamental process parameters, including print speed and gauge pressure. Designers can use this model as starting point to select the required process parameters for the desired track width that can be manually fine-tuned during fabrication to account for any inaccuracies in the model. However, it is suggested that the track width model cannot account for a special case of over-extrusion and designers should avoid predicted track widths significantly larger than the nozzle diameter.

4. Finally, the development and characterization of an embedded PANI-based piezoresistive strain sensor was conducted. Through application of the multi-material CNC extrusion system the sensor was fabricated by concurrent deposition of a flexible TPE support material and the embedded active PANI-DBSA structure. The sensor performance and stability was evaluated under cyclic longitudinal loading. These tests demonstrated that after initial cycling the sensor performance begins to stabilize and exhibits gauge factors in a similar order to previously reported results.

6.2 Summary of contributions

The most significant research contributions presented in this thesis are summarized as follows:

- The first-ever study of the counterion-induced thermal doping method of PANI for

the application of AM. Characterization of the PANI-DBSA paste flow properties yielding an empirical model to describe the paste shear-thinning behaviour as a function of thermal doping time.

- A novel apparatus for the AM of high-resolution conductive 3D PANI structures. Through integration of a conventional FFF delta robot with a paste extrusion system the concurrent deposition of fluid-based materials and conventional filament-based materials has been achieved. This apparatus not only allows for the fabrication of complex, high-resolution 3D conductive PANI structures but also enables transducer fabrication by embedding active materials in a passive support structure.

- Adaptation of a model for the DIW of bioinks to the application of PANI-based paste extrusion. This model incorporates key process parameters and material properties to allow designers to tune the fabrication process with application specific parameters. The model predicts the extruded track width based upon material flow properties and process parameters such as print speed, nozzle diameter, and extrusion pressure.

- The first-ever example of the in-situ embedding of a PANI-based sensor by AM techniques. This sensor capitalizes on the piezoresistivity of PANI to embed the active material in a flexible TPE support to create a compliant sensor that demonstrates potential as a practical application of this new fabrication system.

6.3 Recommendations for future research

The rheological study presented in this thesis provides an insight into the effect of the thermal doping process on the rheological properties of the paste. However, this study focused on thermal doping conducted at 100 °C for a range of times. A future study

investigating the effect of thermal doping temperature on paste properties would be valuable and could further elucidate the optimal processing parameters of PANI-DBSA for AM techniques. Additionally, a transition in measurement equipment to measure the heat transfer in the paste mixing system would allow the development of a thermal doping model that could be scaled to any batch size.

The multi-material extrusion system in combination with counterion-induced thermal doping overcomes previous limitations to the realization of 3D PANI structures. This system may be improved through the addition of in-situ thermal doping. If heat is applied directly at the nozzle, the post-extrusion thermal doping process may be eliminated. There may also be an improvement in the quality of the achievable structures. For example, if a high-degree of doping is achieved at the nozzle, the extruded paste may be near solid, improving its mechanical properties for the realization of high aspect ratios, overhangs, and bridges.

The strain sensor study provided initial information towards the piezeoresistive response of the PANI-based sensors. This study could benefit from a longer cycling period to investigate the long-term stability of the devices and assess any temporal effects. This study also investigated the effect of post-fabrication thermal doping times on the piezoresistive response, however another meaningful study may be to explore the change in mechanical and electrical properties of the PANI-DBSA complex as a function of post-fabrication thermal doping time and temperature.

One of the key advantages of this system is the design freedom enabled by the AM workflow and fabrication apparatus. As such, more complex sensor designs should be investigated to improve performance. For example, new sensor designs could aim to resolve strains applied in multiple directions, or contain multi-layered embedded elements to analyze the pressure field throughout the structure.

Appendices

Appendix A

Software code listing

A.1 Steps per mm converter python script

```
import sys, fileinput, re
import tkinter as tk
from tkinter import filedialog

# Get the user to input the source file for conversion
root = tk.Tk()
root.withdraw()
filename = filedialog.askopenfilename()

# Get the number of tools in the file
print('How many tools are in the target file?')
num_tools = int(input())
extrude_speed = [0] * num_tools

# Get the steps per mm of each tool
for i in range(0,num_tools):
    print('Input E steps per mm for tool ' + str(i))
    extrude_speed[i] = float(input())

# Rewrite each line of the input file.
for line in fileinput.input(filename, inplace=1):
    sys.stdout.write(line)
    if re.search('^T[0-9]', line):
        i = int(line[1])
        if i >= 0 and i < len(extrude_speed):
        sys.stdout.write('M92 E' + str(extrude_speed[i]) + '\n')

print('Conversion done!')
```

steps.py

A.2 Stepper motor to Ultimus V signal conversion

```
#define STEP 2
#define AL 5
#define DIR 3
#define OUT 4
#define LED 13
#define DISPENSE_TIME 25000
#define MIN_WAIT_TIME 10000

volatile long dispense_delay, wait_delay;
long last_time, dt;
bool out, last_out;

void setup() {
  pinMode(STEP, INPUT_PULLUP);
  pinMode(AL, INPUT_PULLUP);
  pinMode(DIR, INPUT_PULLUP);
  pinMode(OUT, OUTPUT);
  pinMode(LED, OUTPUT);
  digitalWrite(OUT, LOW);
  attachInterrupt(digitalPinToInterrupt(STEP), step_rise, RISING);
  last_time = micros();
}

void loop() {
  dt = micros() - last_time;
  last_time = micros();
  out = digitalRead(AL) && !digitalRead(DIR);

  if (dispense_delay > 0)
    dispense_delay -= dt;
  else
    out = false;

  if (wait_delay > 0) {
    wait_delay -= dt;
    out = false;
  }

  if (last_out != out) {
    digitalWrite(OUT, out);
    digitalWrite(LED, out);
    if (last_out) wait_delay = MIN_WAIT_TIME;
    last_out = out;
  }
}

void step_rise() {
  dispense_delay = DISPENSE_TIME;
}
```

Dispense_Communicator.ino

Appendix B

Curriculum Vitae

Name:	Frederick Benjamin Holness
Post-Secondary Education and Degrees:	The University of Western Ontario London, Ontario, Canada 2011 – 2015 B.E.Sc. Mechanical Engineering
Honours and Awards:	NSERC Canada Graduate Scholarship - Master's Program 2016 – 2017 Province of Ontario Graduate Scholarship (declined) 2016 – 2017 NSERC Canada Graduate Scholarship - Doctoral (accepted) 2017 – 2020 The University of Western Ontario Dean's Honour List 2012, 2013, 2014, 2015
Related Work Experience:	Teaching Assistant The University of Western Ontario MME 4450a - Control Systems: Theory and Practice 2015 – 2016 Teaching Assistant The University of Western Ontario MME 3350b - System Modelling and Control 2016 – 2017

Publications:

1. **F. B. Holness** and A. D. Price. Robotic extrusion processes for direct ink writing of 3D conductive polyaniline structures. In Y. Bar-Cohen and F. Vidal, editors, *Electroactive Polymer Actuators and Devices (EAPAD) 2016, SPIE Smart Structures and Materials + Nondestructive Evaluation and Health Monitoring*, volume 9798, pages 97981G–97981G–8. SPIE, 2016.

2. **F. B. Holness** and A. D. Price. Design and fabrication of conductive polyaniline transducers via computer controlled direct ink writing. In Y. Bar-Cohen, editor, *Electroactive Polymer Actuators and Devices (EAPAD) 2017, SPIE Smart Structures and Materials + Nondestructive Evaluation and Health Monitoring*, volume 10163, pages 101632O–101632O–8. SPIE, 2017.

3. C. Micolini, **F. B. Holness**, J. A. Johnson, and A. D. Price. Conductive polymer sensor arrays for smart orthopaedic implants. In V. K. Varadan, editor, *Nanosensors, Biosensors, Info-Tech Sensors and 3D Systems 2017, SPIE Smart Structures and Materials + Nondestructive Evaluation and Health Monitoring*, volume 10167, pages 101670D–101670D–7. SPIE, 2017.

4. **F. B. Holness** and A. D. Price. Direct ink writing of 3D conductive polyaniline structures and rheological modelling. *Smart Materials and Structures*, submitted 2017, currently under review (SMS-105446).

5. C. Micolini, **F. B. Holness**, J. A. Johnson, and A. D. Price. Embedded Conjugated Polymer Sensor Arrays for Load Transmission Measurement in Orthopaedic Implants. *Sensors, Special issue: Force and Pressure Based Sensing Medical Applications*, submitted 2017, currently under review (sensors-218949).